Inorganic Chemistry **2020**, *59*, 14679–14695

Forum Article in the Special Issue: Light-Controlled Reactivity of Metal Complexes

Guest Editors : Prof. Katja Heinze and Prof. Oliver Wenger

DOI: 10.1021/acs.inorgchem.0c01843

Theoretical study of the full photosolvolysis mechanism of $[Ru(bpy)_3]^{2+}$: providing a general mechanistic road map for the photochemistry of $[Ru(N\hat{}N)_3]^{2+}$-type complexes towards both *cis* and *trans* photoproducts.

Adrien Soupart,[#] Fabienne Alary,[#] Jean-Louis Heully,[#] Paul I. P. Elliott,[§*] and Isabelle M. Dixon[#*]

[#]Laboratoire de Chimie et Physique Quantiques, Université de Toulouse, CNRS, 118 route de Narbonne, 31062 Toulouse, France.

[§]Department of Chemistry and Centre for Functional Materials, University of Huddersfield, Queensgate, Huddersfield, HD1 3DH, UK.

Abstract

A complete mechanistic picture for the photochemical release of bpy from the archetypal complex $[Ru(bpy)_3]^{2+}$ is presented for the first time following the description of the ground and lowest triplet potential energy surfaces, as well as their key crossing points, involved in successive elementary steps along pathways towards *cis*- and *trans*-$[Ru(bpy)_2(NCMe)_2]^{2+}$. This work accounts for two main pathways that are identified involving a) two successive photochemical reactions for photodechelation followed by photorelease of a monodentate bpy ligand, and b) a novel one-photon mechanism in which initial photoexcitation is followed by dechelation, solvent coordination and bpy release processes, all of which occur sequentially within the triplet excited state

manifold before final relaxation to the singlet state and formation of final photoproducts. For the reaction between photoexcited $[Ru(bpy)_3]^{2+}$ and acetonitrile, which is taken as a model reaction, pathways towards *cis* and *trans* photoproducts are uphill processes, in line with the comparative inertness of the complex in this solvent. Factors involving the nature of the departing ligand and retained 'spectator' ligands are considered, and their role in selecting mechanistic pathways involving overall two sequential photon absorptions versus one photon absorption for the formation of both *cis* or *trans* photoproducts are discussed in relation to notable examples from the literature. This study ultimately provides a generalised road map of accessible photoproductive pathways for light-induced reactivity mechanisms of photolabile $[Ru(N^N)(N^N')(N^N'')]^{2+}$-type complexes.

Introduction

Ruthenium coordination compounds have a long and remarkable history in inorganic photochemistry. Since the early 1970s, fundamental knowledge has been gained on their photophysical properties, with particularly monumental contributions from the USA (e.g. from the groups of Adamson,[1,2] Crosby,[3,4,5,6,7] Demas,[8,9,10] Endicott[11,12] Wrighton,[13] Meyer,[14,15] Watts,[16] or Sutin,[17,18,19,20]) and Italy.[21,22,23,24] Since then, thousands of derivatives have found numerous applications including in water splitting,[25,26,27] dye-sensitised solar cells,[28,29] as sensitisers for photocatalysis,[30,31] or as sensors or probes for biology.[32] What makes these compounds especially powerful is the tremendous tuning of their properties resulting from chemists' endless creativity.[33,34,35,36,37] Because photoinstability issues are deleterious to photophysical applications,[38,39] the same period has also witnessed thorough photoreactivity studies with a variety of starting compounds and incoming ligands (e.g. anions, coordinating solvents).[40,41,42,43,44,45,46,47] Synthetic applications of photosubstitution reactions followed shortly afterwards[48,49,50,51,52,53,54] and, more recently, applications in phototriggered molecular machines[55,56] or the photorelease of biologically active molecules.[57,58,59,60,61,32,62,63,64] As a continuation to Adamson's formulation of empirical rules regarding relative efficiency and selectivity of photoreactions,[65] several theoretical studies were published in the 1970s with the aim of rationalizing their outcome. Orbital and symmetry considerations have brought up enlightening mechanistic information, initially around Cr(III) and Co(III) photochemistry[66,67,68] and which was then generalized.[69,70,71,72] More recently, the parallel

development of advanced quantum and ultrafast time-resolved spectroscopic methods has enabled an in-depth study of microscopic ligand photorelease mechanisms.[73,74]

Returning to ruthenium, the source of the fascinating properties of this family of complexes, especially its polypyridine derivatives, is found in their triplet excited states, particularly in the metal-to-ligand charge transfer (^{3}MLCT) state, and its rival brother, the ligand-field metal-centered (^{3}MC) state. Both excited states are antagonistic in the sense that the former is capable of photoluminescence and photoinduced electron or energy transfer,[75] whereas the latter undermines these properties and is involved in nonradiative deactivation and photoinstability issues,[42] as beautifully demonstrated for other metal complexes.[76,77] Tuning the relative energies of the ^{3}MLCT and ^{3}MC states is thus of utmost importance in driving the properties of complexes towards the one or other desired regime.[78] Following the first optimisation of a ^{3}MC state in a ruthenium complex (a hexacoordinate $[Ru(bpy)_3]^{2+}$ excited state exhibiting two elongated and mutually trans Ru-N bonds that we term a 'classical' ^{3}MC state),[79] several theoretical mechanistic studies focused on the photoinduced release of a monodentate ligand.[80,81,82,83,84,85,86] Our group initially became interested in photorelease mechanisms involving the loss of a thioether monodentate ligand in collaboration with Bonnet's group.[87] We hypothesised the involvement of ^{3}MC states distinct from those we originally described: these new states display quasi pentacoordinated geometries and are local minima on the lowest triplet potential energy surface (^{3}PES). We proposed that triplet/singlet surface crossings in the region of the local ^{3}MC minima were mechanistically determining, crossing with the reactant ^{1}PES for the classical ^{3}MC state vs crossing with the product ^{1}PES for the quasi pentacoordinated ^{3}MC state.[88] From this viewpoint, the ease of population of this latter ^{3}MC state can be correlated to the experimental photosubstitution quantum yield.

Bidentate ligand photorelease has been explored in recent years in view of biological applications.[89,90,91,92,93,94,95,96,97,98] A two-step mechanism was inferred from early spectroscopic observations invoking an intermediate containing a monocoordinated bidentate ligand (Scheme 1).[45,49,50,99,100,101,102,103,104] Structural characterisation of such κ^1 intermediate photoproducts has been provided by ^{1}H-NMR spectroscopy[105,106,107,108,109] and X-ray diffraction studies.[110] Note that the reaction coordinate for stepwise bidentate ligand loss is inevitably more complex than the corresponding one for monodentate ligand loss. Building up on the mechanistic hypothesis for-

mulated in 2016 (different roles played by distinct ^{3}MC states),[88] we embarked on the theoretical mechanistic study of photoinduced bidentate ligand loss in collaboration with Elliott's group.[111,105,110] Novel ^{3}MC states were characterised, displaying either hexacoordinate classical (*trans* Ru-N elongation) or flattened (involving elongation of two cis Ru-N bonds) hexa- and pentacoordinate geometries.[112] This study reinforced our conviction that surface crossings with reactant or product ^{1}PES were crucial in determining the outcome of a photochemical reaction. As a side hypothesis, we also envisaged reaction in the triplet state, bypassing surface crossing to the ^{1}PES of the κ^1 intermediate photoproduct and directly populating the ^{3}MLCT state of the κ^1-bound species. The efficiency of this path is certainly moderate as it involves energy barriers around 20 kcal/mol.[113] Finally, the recent identification of a second, flattened ^{3}MC state for $[Ru(bpy)_3]^{2+}$, that we consider more prone to ligand loss than the classical ^{3}MC state of the type described above,[114] has prompted us to attempt to generalise the proposed mechanism for bidentate ligand loss.[115] In this work we thus sought to establish a general ligand photorelease mechanistic framework in agreement with all the available experimental data, i.e. stepwise mechanisms through a commonly invoked κ^1 intermediate photoproduct as well as concerted excited state mechanisms directly yielding final *cis* and *trans* photoproducts without involving κ^1 ground state intermediate.[54] Note that photoisomerisation issues (Δ/Λ[116,117] and *cis-trans* isomerisations[118,119]) are outside of the scope of this work.

Scheme 1. General mechanistic picture for 2-step bidentate ligand loss and coordination of two solvent molecules (**S**) onto a metallic complex [M].

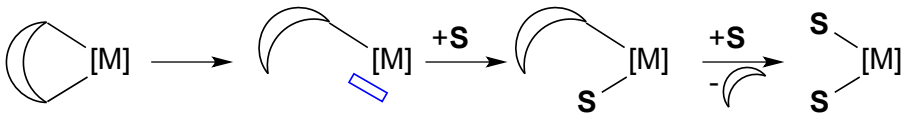

Methodology

The reaction investigated in this work involves $[Ru(bpy)_3]^{2+}$ as reactant despite other Ru(II) complexes being much more photoreactive with their photolysis products formed in much higher quantum yield.[120,121,122,123,124] Whilst $[Ru(bpy)_3]^{2+}$ is by comparison largely photoinert in acetoni-

trile,[49] the photosolvolysis of this benchmark archetypal complex can be used as a highly informative model reaction that builds upon the results of our previous work. Concepts and understanding from this work may then be translated to other systems exhibiting greater photoreactive efficiency. Regarding the choice of coordinating solvent, acetonitrile indeed bears several advantages over the commonly encountered water, in that proton transfer, pH and H-bonding issues are avoided. Acetonitrile is a neutral ligand that allows charge conservation throughout the whole process (all complexes are dicationic and all free ligands are neutral). It bears a single coordinating lone pair giving rise to directional coordination, which facilitates the search for new structures. For all these reasons we considered that the approximation of successively reacting two individual MeCN molecules with $[Ru(bpy)_3]^{2+}$ in implicit MeCN (polarisable continuum model) is an acceptable model that should provide us with general mechanistic information in relation to bidentate ligand loss. As both *cis*- and *trans*-$[Ru(bpy)_2L_2]^{2+}$ products are known, we envisaged forming *cis*-$[Ru(bpy)_2(NCMe)_2]^{2+}$ and *trans*-$[Ru(bpy)_2(NCMe)_2]^{2+}$. *cis*-$[Ru(bpy)_2(NCMe)_2]^{2+}$ is indeed the photosolvolysis product formed from $Ru(bpy)_2(btz)^{2+}$ (btz = 1,1'-dibenzyl-4,4'-bi-1,2,3-triazolyl)[125] or $[Ru(bpy)_2(inv\text{-}pytri)]^{2+}$ (inv-pytri = 2-(1H-1,2,3-triazol-1-yl)pyridine),[126,109] for example. The mechanism we are proposing is split into elementary steps, each of these involving well-defined singlet and triplet minima. The topology of the ^{1}PES and ^{3}PES is also described through the determination of energy barriers from minimum energy path calculations (NEB, nudged elastic band) complemented by the optimisation of singlet-triplet crossings (MECP, minimum energy crossing points), at the B3LYP[127,128]-D3BJ[129,130]/def2-ECP[131]/def2-TZVP(-f)[132] level of theory. Four successive regions, shown with different background colors in the schemes in this article, are defined as a function of the coordination sphere of the metal : $(bpy)_3$; $(bpy)_2(\kappa^1\text{-bpy})$; $(bpy)_2(\kappa^1\text{-bpy})(MeCN)$; $(bpy)_2(MeCN)$; $(bpy)_2(MeCN)_2$. The border zones between these regions (diffusion of the released ligand and coordination of the incoming ligand) are explored through NEB calculations, a method which we exploit here as powerful relaxed surface scans that do not require the (user-dependent) numerical definition of the reaction coordinate through geometrical parameters. The optimisation of minima and minimum energy paths has enabled us to construct singlet and triplet potential energy surfaces. Following the description of the key protagonists, we report full mechanisms for the formation of *cis* and *trans*-$[Ru(bpy)_2(NCMe)_2]^{2+}$ and provide discussion around possible connections between these pathways. The results presented offer fundamental insights, not only for the photochemical properties

and processes for $[Ru(bpy)_3]^{2+}$ under investigation but can be translated to the myriad photoactive complexes known in the literature.

Results and discussion

In the nomenclature used herein (Table 1), the complexes (singlet ground states and triplet excited states) were named as a function of the ligands in the coordination sphere (A for acetonitrile, B for bipyridine) : B_3 when 3 bpy ligands are bound to the metal, κ^1-B_3 when one bpy ligand is monodentate (pentacoordinate species), κ^1-B_3A_1 when one bpy ligand is monodentate and one NCMe molecule has been coordinated (primary photoproducts), B_2A_1 following the loss of one bpy ligand (pentacoordinate species), and finally B_2A_2 in the final photoproducts. In addition, (pro-)*cis* and (pro-)*trans* prefixes have been used to specify the relative positions of the κ^1-bpy/vacancy or NCMe/vacancy (for pentacoordinate species), or the relative positions of the κ^1-bpy/NCMe or NCMe/NCMe sites (for hexacoordinate species). Singlet and triplet states have been optimised, as well as singlet/triplet minimum energy crossing points (MECPs). All energies are given relative to the energy of $[Ru(bpy)_3]^{2+}$ + 2 MeCN isolated molecules computed in COSMO-SMD acetonitrile. The numbering scheme is shown on Figure 1.

Figure 1. Numbering scheme used in this study for coordinating N-atoms in $[Ru(bpy)_3]^{2+}$.

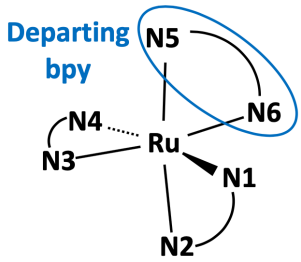

Table 1. Abbreviations used throughout this work. All states can be derived as *cis* or *trans* isomers, with singlet or triplet spin multiplicity.

abbreviation	formula
B_3	$[Ru(bpy)_3]^{2+}$
κ^1-B_3	$[Ru(\kappa^1\text{-bpy})(bpy)_2]^{2+}$
κ^1-B_3A_1	$[Ru(\kappa^1\text{-bpy})(bpy)_2(NCMe)]^{2+}$
B_2A_1+B	$[Ru(bpy)_2(NCMe)]^{2+}$+bpy (adduct)
B_2A_1	$[Ru(bpy)_2(NCMe)]^{2+}$
B_2A_2	$[Ru(bpy)_2(NCMe)_2]^{2+}$

1. Topologies of the *cis* singlet PES and *trans* singlet PES

Photochemical ligand release may involve the participation of a sequence of both singlet ground state and triplet excited state species. It is thus imperative to throughly characterise the singlet potential energy surface between the reactant and final photoproducts and capture these important intermediate species. Experimental studies conclude that *cis*- and *trans*-bis(solvento) adducts can be formed from prolonged photolysis of $[Ru(bpy)_3]^{2+}$, the *cis* product being the major isomer. Similarly to what had been observed for osmium,[106] primary photoproducts bearing one monodentate bpy ligand and one bound solvent molecule could be formed as *cis* or *trans* isomers too. Thus each of the singlet PES for the formation of *cis* and *trans*-$[Ru(bpy)_2(NCMe)_2]^{2+}$ should have three local minima of general formula B_3, κ^1-B_3A_1 and B_2A_2. If one assumes a dissociative mechanism this implies that photoreactivity proceeds through formally pentacoordinate intermediates along the reaction path. This means that each singlet PES should also have two local minima of general formula κ^1-B_3 and B_2A_1. In addition to B_3-GS, minima have been located and geometries optimised for the two hexacoordinate species κ^1-B_3A_1-GS and B_2A_2-GS and two pentacoordinate species κ^1-B_3-GS and B_2A_1-GS along the PES for the formation of both the *cis* and *trans* products. Finally, upon diffusion of the departing bpy ligand, one may envisage van der Waals adducts, which were also searched for and optimised (B_2A_1+B structures). If these structures exist, many isoenergetic conformers can be expected, only one of which is presented here. The van der Waals B_2A_1+B adducts are found about 10 kcal/mol higher in energy than their corresponding κ^1-

B_3A_1 species. The geometries for all these closed shell ground state species are depicted in Figure 2 with key structural parameters presented in Table 2.

The shortest Ru-N bond is always found *trans* to the vacancy in pentacoordinate intermediate species (Ru-N3 in *cis*-κ^1-B_3-GS; Ru-N6 in *trans*-κ^1-B_3-GS; Ru-N2 in *cis*-B_2A_1-GS; Ru-NCMe in *trans*-B_2A_1-GS) or *trans* to the departing bpy in the van der Waals adducts (Ru-N2 in *cis*-B_2A_1-GS+B; Ru-NCMe in *trans*-B_2A_1-GS+B). In the κ^1-B_3 species, a significant dihedral angle between the two rings of the κ^1-bound bpy is found (>70°). In each pentacoordinate ground state species, we note the opening of a quadrant that allows the incoming ligand to approach : 165° in *cis*-κ^1-B_3-GS (Fig. S4) ; 153° in *trans*-κ^1-B_3-GS (Fig. S9) ; 175° in *cis*-B_2A_1-GS (Fig. S7) ; 164° in *trans*-B_2A_1-GS (Fig. S12). Structurally speaking, the removal of the κ^1-bound bpy is accompanied by significant elongation of all Ru-pyridine distances in the van der Waals adducts (Fig. S6 and S11). Classical Ru-N distances are restored (Fig. S7 and S12) in the subsequent pentacoordinate B_2A_1-GS minima, which are located a further 25-30 kcal/mol higher in energy. It is noteworthy that some differences persist between the *cis* and *trans* GS structures, the *trans* isomer always displaying shorter Ru-acetonitrile and longer Ru-pyridine distances, in line with the strain caused by the two bipyridine ligands being approximately coplanar with one another.

The topologies of the *cis* and *trans* ^{1}PESs shown in Figure 2 were constructed by connecting optimised minima through minimum energy paths obtained from Nudged Elastic Band calculations (Supporting Information). Several experimental observations can lead us through the discussion. First of all, $[Ru(bpy)_3]^{2+}$ is kinetically inert, in line with the fact that the computed energy barrier for thermal dechelation of bpy (B_3-GS towards κ^1-B_3-GS, *ca* 50 kcal/mol) is too high to be overcome under normal reaction conditions. Formal loss of the monodentate bpy ligand from the intermediate species *cis*- and *trans*-κ^1-B_3A_1-GS to form the pentacoordinate species *cis*- and *trans*-B_2A_1-GS also require surmounting significant energy differences (*via* their van der Waals adducts) of 35 and 38 kcal/mol respectively. Whilst loss of the bpy ligand clearly requires photochemical initiation, the results suggest that, if the singlet state solvent intermediates κ^1-B_3A_1-GS are formed in the course of the ligand loss process, absorption of a second photon will be required at this mid-point. In agreement with the favoured formation of the *cis*-B_2A_2 isomer, all minima on the *cis* ^{1}PES are found to be lower in energy than their *trans* counterparts by 6-12 kcal/mol.

Table 2 : Ru-N distances (Å) and selected angles for closed-shell minima leading to *cis*-$[Ru(bpy)_2(NCMe)_2]^{2+}$ and *trans*-$[Ru(bpy)_2(NCMe)_2]^{2+}$ (Ru-N = 2.07-2.08 Å in B_3-GS).

	cis-κ^1-B_3	*cis*-κ^1-B_3A_1	*cis*-B_2A_1+B	*cis*-B_2A_1	*cis*-B_2A_2
Ru-N1	2.085	2.086	2.175	2.065	2.077
Ru-N2	2.067	2.071	2.086	1.990	2.062
Ru-N3	1.986	2.058	2.179	2.066	2.070
Ru-N4	2.060	2.067	2.177	2.083	2.078
Ru-N5	3.828	3.993	3.852	-	-
Ru-N6	2.112	2.173	2.634	-	-
$Ru\text{-}NCMe_a$	-	2.038	2.039	2.026	2.030
$Ru\text{-}NCMe_b$	-	-	-	-	2.032
angle	N5-C-C-N6 70° N2-Ru-N6 165°	N5-C-C-N6 83°	N5-C-C-N6 51°	N3-Ru-N5 175°	-
	trans-κ^1-B_3	*trans*-κ^1-B_3A_1	*trans*-B_2A_1+B	*trans*-B_2A_1	*trans*-B_2A_2
Ru-N1	2.107	2.089	2.183	2.090	2.090
Ru-N2	2.123	2.105	2.166	2.112	2.111
Ru-N3	2.148	2.125	2.246	2.123	2.115
Ru-N4	2.128	2.095	2.167	2.108	2.110
Ru-N5	3.644	3.764	3.773	-	-
Ru-N6	2.068	2.155	2.528	-	-
$Ru\text{-}NCMe_a$	-	2.022	1.985	1.930	2.016
$Ru\text{-}NCMe_b$	-	-	-	-	2.019
angle	N5-C-C-N6 73° N2-Ru-N3 153°	N5-C-C-N6 71°	N5-C-C-N6 58°	N1-Ru-N4 164°	-

Figure 2. Singlet potential energy profile towards *cis*-$[Ru(bpy)_2(NCMe)_2]^{2+}$ (top) and *trans*-$[Ru(bpy)_2(NCMe)_2]^{2+}$ (bottom).

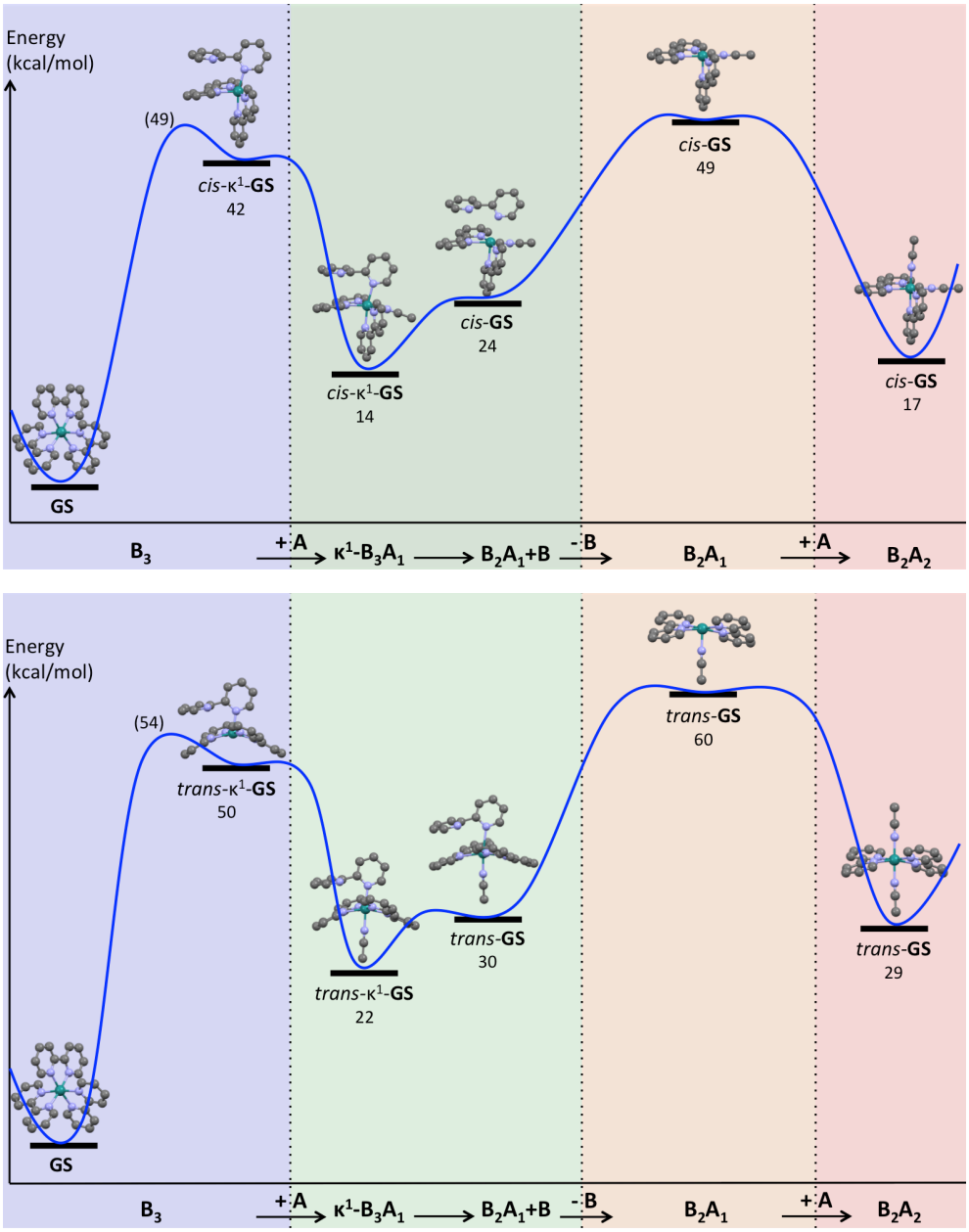

2. Bringing in the triplet PES : a tale of two sequential photochemical reactions

The energy barriers for both the initial bpy dechelation and subsequent formal dissociation are rather high and therefore preclude that either of these steps is thermally mediated. We therefore proceed to examine the photochemical route, bringing into consideration the evolution of the

complex within the triplet manifold. In the following sections we examine the photochemical initiation, dechelation and solvation to form the ground state intermediate κ^1-B_3A_1 and subsequent photochemical bpy loss and second solvation to form B_2A_2 for the two sequential photon-driven mechanisms for both *cis* and *trans* product formation. The sequence of elementary steps connecting relevant excited and ground state species are depicted in Scheme 2 for the *cis* and *trans* product formation routes respectively. Table 3 summarises the main geometrical parameters for the triplet states involved along these paths.

Ruthenium polypyridine complexes display strong ^{1}MLCT-based absorption bands in the visible region, a specificity that makes them amenable to application as dyes for solar cells, sensors and probes, or as photosensitisers.[29,133,134,32] Following light absorption that populates several ^{1}MLCT states, ultrafast intersystem crossing occurs to populate ^{3}MLCT states. According to Kasha's rule, luminescence could occur from the lowest of these, but higher lying ^{3}MLCT states could also be populated and could decay to various other triplet states by internal conversion processes.[135] We have previously reported two distinct ^{3}MC states for $[Ru(bpy)_3]^{2+}$ having a different hole and particle pair, which we then termed $^3MC_{trans}$ and $^3MC_{cis}$ (*cis* and *trans* suffixes, in this context, refer to the positions of the elongated Ru-N bonds: two Ru-N bonds to distinct bpy ligands for $^3MC_{trans}$ vs. both Ru-N bonds to the same bpy ligand in $^3MC_{cis}$).[114] The singly occupied orbital hosting the particle is especially distinctive, being d_{z2}-like for $^3MC_{trans}$ and d_{x2-y2}-like for $^3MC_{cis}$. Thus, we can expect the population of these states to occur efficiently from distinct ^{3}MLCT states. In this respect, careful inspection of TD-DFT calculations can inform us on the localisation and energy of these states at the ground state geometry. Time dependent DFT at the B_3-GS geometry (Table S1) shows that the three lowest ^{3}MLCT states (T_1-T_3, 2.43–2.45 eV) share the same hole as B_3-$^3MC_{trans}$, whereas states T_4-T_9 (2.49–2.71 eV) share the same hole as B_3-$^3MC_{cis}$. Given the energetic proximity of these states, one can suppose several of them be involved in the system's relaxation cascade, allowing the population of several ^{3}MC states from the ^{3}MLCT manifold.

2.1 The first photochemical event : bpy dechelation

Identification and characterisation of ^{3}MC states undoubtedly represents the most demanding part of this kind of study. We have previously shown how crucial they are in photolabilisation mechanisms,[88,112] where they can be considered as pre-dissociated states. As such, they are worthy of devoting most of the human and computing resources to. Structural distortions due to the occupation of antibonding metal-ligand dσ* orbitals (bond elongations, angular distortions) are such in ^{3}MC states that at these geometries the ground state is strongly destabilised, resulting in singlet/triplet crossing regions in the neighbourhood of ^{3}MC minima. The optimisation of minimum energy crossing points (MECP)[136,137] is therefore systematically performed here and the orbital parentage with the parent ^{3}MC minimum is verified.

Starting from the previously described $^3MC_{trans}$ and $^3MC_{cis}$ states,[114] the $^3MC_{trans}$ state becomes B_3-$^3MC_{trans}$ in the current nomenclature and corresponds to the original ^{3}MC state characterised by population of a d_z^2-like dσ* orbital.[79] Given that the bond elongations in this state are towards two different bpy ligands, this state is considered *not* to be directly involved in the photoinduced ligand loss mechanism. On the other hand, $^3MC_{cis}$, which we had estimated to be more predicated to ligand loss (as it repelled both coordinating atoms of a single bpy ligand) is here termed B_3-$^3MC_{cis}$. In this new study we have been able to refine its description further and have been able to optimise two conformers (identical electronic states according to their singly occupied molecular orbitals) which display an open quadrant[138] (which $^3MC_{trans}$ does not have). One could view these two conformers (Figure 3) as predisposing the complex to coordination by solvent in a manner which could lead onwards either to the *cis* product (called pro-*cis*-B_3-$^3MC_{cis}$ as the open quadrant is adjacent to the κ^1-bpy ligand; N2-Ru-N6 = 128°) or to the *trans* product (called pro-*trans*-B_3-$^3MC_{cis}$ as the open quadrant lies *trans* to the κ^1-bpy ligand; N2-Ru-N3 = 121°). The energy barrier on the minimum energy path from the lowest ^{3}MLCT state to either of these states is similar at 10-12 kcal/mol (Fig. S47 and S54). The optimised geometries of each of these conformers leads us to their MECPs (pro-*cis*-B_3-$MECP_{cis}$ and pro-*trans*-B_3-$MECP_{cis}$) that were also found separately from the corresponding κ^1-B_3-GS species (*cis*-κ^1-B_3-GS and *trans*-κ^1-B_3-GS). This is therefore a strong indication that the conformation of the B_3-$^3MC_{cis}$ state is decisive in driving the system towards either the *cis* or *trans*-κ^1-B_3A_1 primary photoproduct.[139,140] We thus connect *cis*-κ^1-B_3-GS with pro-*cis*-$MECP_{cis}$, itself connecting with pro-*cis*-B_3-$^3MC_{cis}$ and similarly, *trans*-κ^1-B_3-GS with pro-*trans*-$MECP_{cis}$ and in turn pro-*trans*-B_3-$^3MC_{cis}$.

Table 3: Ru-N distances (Å) and selected angles for triplet minima leading to *cis*- and *trans*-$[Ru(bpy)_2(NCMe)_2]^{2+}$.

	pro-*cis*-B_3 $^3MC_{cis}$	*cis*-κ^1-B_3A_1 ^{3}MLCT	*cis*-B_2A_1+B ^{3}MC	*cis*-B_2A_1 ^{3}MC
Ru-N1	2.106	2.107	2.133	2.116
Ru-N2	2.300	2.072	2.344	2.260
Ru-N3	2.215	2.014	2.060	2.068
Ru-N4	2.088	2.042	2.063	2.063
Ru-N5	2.547	3.899	3.825	-
Ru-N6	2.162	2.156	2.815	-
Ru-$NCMe_a$	-	2.087	2.047	2.045
angle	N2-Ru-N6 128°	N5-C-C-N6 71°	N5-C-C-N6 30°	N3-Ru-$NCMe_a$ 174°
	pro-*trans*-B_3 $^3MC_{cis}$ [a]	*trans*-κ^1-B_3A_1 ^{3}MLCT	*trans*-B_2A_1+B ^{3}MC	*trans*-B_2A_1 ^{3}MC
Ru-N1	2.078	2.049	2.136	2.185
Ru-N2	2.177	2.057	2.080	2.081
Ru-N3	2.135	2.118	2.080	2.070
Ru-N4	2.080	2.110	2.094	2.071
Ru-N5	2.530	3.593	3.773	-
Ru-N6	2.384	2.132	3.347	-
Ru-$NCMe_a$	-	2.055	2.196	2.086
angle	N2-Ru-N3 121°	N5-C-C-N6 59°	N1-Ru-N4 129° N4-Ru-$NCMe_a$ 141° N5-C-C-N6 18°	N1-Ru-N4 120° N4-Ru-$NCMe_a$ 141°

[a] From ref [114].

Scheme 2. Proposed multistep productive mechanism towards *cis*-$[Ru(bpy)_2(NCMe)_2]^{2+}$ (top) and *trans*-$[Ru(bpy)_2(NCMe)_2]^{2+}$ (bottom) involving two sequential photochemical steps.

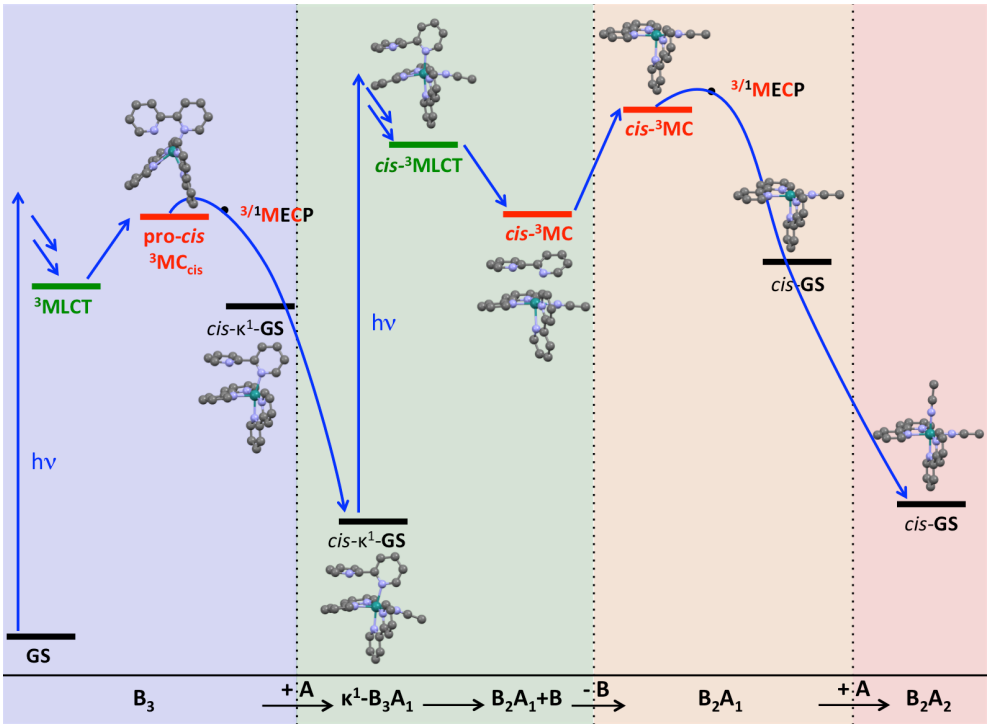
3MLCT
hν
GS
pro-cis
3MC$_{cis}$
3/1MECP
cis-κ1-GS
cis-3MLCT
hν
cis-κ1-GS
cis-3MC
3/1MECP
cis-3MC
cis-GS
cis-GS
B3
+A
κ1-B3A1
B2A1+B
-B
B2A1
+A
B2A2

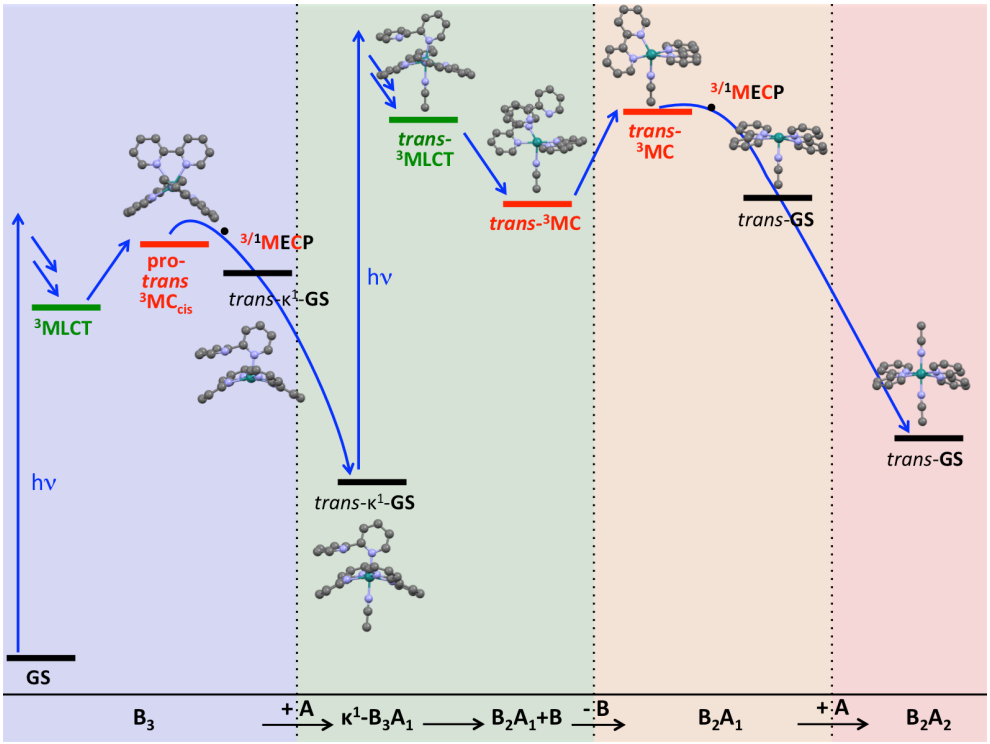
3MLCT
hν
GS
pro-
trans
3MC$_{cis}$
3/1MECP
trans-κ1-GS
trans-
3MLCT
hν
trans-κ1-GS
trans-3MC
3/1MECP
trans-
3MC
trans-GS
trans-GS
B3
+A
κ1-B3A1
B2A1+B
-B
B2A1
+A
B2A2

Figure 3. Structures of pro-*cis*-B_3-$^3MC_{cis}$ (left) and pro-*trans*-B_3-$^3MC_{cis}$ (right), highlighting their respective open quadrant that will facilitate the approach of incoming MeCN.

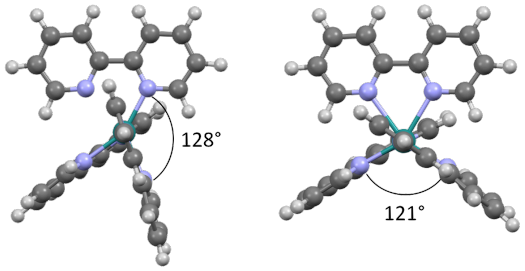

2.2 First solvation : quenching the κ^1-B_3-GS species with acetonitrile

Following the population of either $^3MC_{cis}$ state (i.e. pro-*cis* or pro-*trans*), each of which bears an open quadrant, a neighbouring MECP is available to relax the system back to the closed-shell singlet PES of a truly pentacoordinate κ^1-B_3-GS species. According to Wigner rules,[140] trapping pentacoordinate singlet closed-shell species with solvent, here to form the intermediate species κ^1-B_3A_1-GS, is a barrierless process (confirmed here in singlet state NEB calculations, Fig. S37 and S42). Further, experiments have pointed to the fast trapping of electrophilic 16-electron species by coordinating solvent.[84,141] The electrophilicity of the metal in the pentacoordinate singlet κ^1-B_3 species is indeed seen in the presence of a low-lying vacant metallic orbital exhibiting a large lobe in the vacated coordination site (Fig. S4 and S9). Coordination of acetonitrile to *cis*/*trans*-κ^1-B_3-GS therefore readily yields the primary photoproducts *cis*/*trans*-κ^1-B_3A_1-GS. Interestingly, the N6 atom that is the coordinating N-atom of the κ^1-bpy ligand migrates from being situated *cis* to N2 in B_3-MLCT to being *trans* to N2 in *cis*-κ^1-B_3-GS, which provides an unhindered coordination site for acetonitrile for the formation of *cis*-κ^1-B_3A_1-GS.

2.3 To go forwards or backwards ? Evolution from the κ^1-B_3A_1 species

Having arrived at the primary photoproduct κ^1-B_3A_1-GS, we have the choice to either release NCMe to reform B_3-GS or move forward towards B_2A_2-GS via van der Waals adducts. Although the computed energy barriers are of the same order of magnitude with our model (30-

40 kcal/mol), experiments[105,110] indicate that the thermal reverse reaction (computed barriers 33 and 31 kcal/mol for the *cis* and *trans* paths respectively, Fig. S38 and S43) is favoured over the forward one (computed barriers 37 and 39 kcal/mol for the *cis* and *trans* paths respectively, Fig. S40 and S45), which makes sense given the spatial proximity of the binding site provided by the chelating ligand. Ring closure of the metallacycle is then favoured over bpy loss.[50] However, just as the high energy barriers for bpy ligand dissociation would disfavour these processes occuring thermally, the energy barriers for going backwards toward B_3-GS are similarly large. We therefore return to a photochemical pathway and evolution of the system on the triplet PES.

Experimental evidence for the existence of intermediate B_3A_1 photoproducts implies that under continuous irradiation, the corresponding B_3A_1-^{3}MLCT states will become involved. We therefore optimised these states and found *cis*-κ^1-B_3A_1-MLCT and *trans*-κ^1-B_3A_1-MLCT to lie 51 and 48 kcal/mol higher in energy than the reference respectively. As with photoexcitation of B_3-GS, light absorption by *cis*/*trans*-κ^1-B_3A_1-GS will populate a number of MLCT states whose internal conversion and relaxation cascade may preferentially lead to population of particular ^{3}MC states. We therefore carried out a similar TD-DFT analysis to that conducted for B_3-GS, at the *cis*-κ^1-B_3A_1-GS geometry (Table S2) and at the *trans*-κ^1-B_3A_1-GS geometry (Table S3). It appears that the hole of the *cis* van der Waals adduct (*cis*-B_2A_1-^{3}MC+B) is the HOMO-2 of *cis*-κ^1-B_3A_1-GS, i.e. it is the same as in T_3, T_5 or T_6 (2.59-2.78 eV) and as in S_5, the most absorbing singlet (2.97 eV). Regarding the *trans* van der Waals adduct (*trans*-B_2A_1-^{3}MC+B), the hole corresponds to the HOMO of *trans*-κ^1-B_3A_1-GS, i.e. it is the same as in T_1 or T_3.

Now in the triplet state, the *cis*/*trans*-κ^1-B_3A_1-MLCT states have the same choice and could either move forward towards bpy loss (productive pathway) or release NCMe and revert to the initial B_3 world (nonproductive pathway). The case of the *trans*-κ^1-B_3A_1-^{3}MLCT state is particularly illustrative of this competition because population of a single dσ* orbital would repel both the half-bound bpy and the newly coordinated MeCN ligand, as they are located *trans* to one another. Following Zink's reasoning,[66,67,68] the Ru-NCMe overlap being larger than the Ru-pyridine overlap in the bonding dσ orbital, one can expect NCMe to be more repelled than pyridine when the corresponding dσ* orbital is populated, i.e. a return to the starting material would be particularly favoured in the *trans* case. This may be one of the reasons why *trans*-B_2A_2 products are less fa-

voured, in various photolysis experiments. For the forward reaction (bpy loss) along the *cis* and *trans* routes we find a minimum in each case represented by a pentacoordinate ^{3}MC state with which the departing bpy ligand is still associated as a van der Waals adduct (*cis*- and *trans*-B_2A_1-^{3}MC+B, Fig. S20 and S31). These adducts are found to be lower in energy by 8 and 12 kcal/mol than their corresponding κ^1-B_3A_1-MLCT state respectively. In *cis*-B_2A_1-MC+B the departing bpy ligand has a significantly elongated Ru-N distance to the N atom of the previously monodentate bpy ligand (Ru-N6 = 2.81 Å). The bpy ligand is significantly inclined with respect to this Ru-N distance, with the other pyridine ring (the decoordinated pyridine ring of the previously κ^1-bpy) engaged in a π-stacking arrangement with one of the retained bpy ligands. In the case of *trans*-B_2A_1-MC+B, the retained bpy ligands undergo a rearrangement process upon conversion from the MLCT state in which one of the ligand tilts up to relieve steric strain (N1-Ru-N4 = 141°, Figure S31). Here, the departing bpy engages in π-stacking with the retained bpy ligand that tilts up towards it. This arrangement interestingly presents a new open quadrant adjacent to the acetonitrile ligand (N4-Ru-NCMe = 129°), the possible significance of which we shall return to later.

NEB calculations were carried out to determine minimum energy paths for both MeCN loss (towards *cis* and *trans*-κ^1-B_3) and bpy loss (towards these van der Waals adducts) from both *cis*- and *trans*-κ^1-B_3A_1-MLCT states. Both forward and reverse energy barriers are small in our calculations (*cis* isomer : forward process 3 kcal/mol (Fig. S48) and backward process 4 kcal/mol (Fig. S50) ; *trans* isomer : forward process 2 kcal/mol (Fig. S55) and backward process 1.5 kcal/mol (Fig. S57)). The general trend of energy barriers being significantly reduced in the excited state is maintained.

2.4 Dissociation of bpy, second solvation and final photoproduct formation

Once the system has reached the van der Waals adducts *cis*- and *trans*-B_2A_1-^{3}MC+B, pulling away bpy to form pentacoordinate B_2A_1-^{3}MC states represents a moderate energy penalty of 13-14 kcal/mol (Fig. S49 and S56) (vs 25-30 kcal/mol in the corresponding singlet states, Fig. S39 bottom and S44 bottom). In the case of *trans*-B_2A_1-MC the relative arrangement of the remaining bpy ligands is retained with one bpy ligand significantly tilted up and away from the acetonitrile ligand. The open pro-*trans* quadrant is consequently much smaller in the resultant *trans*-B_2A_1-

^{3}MC (120°, Fig. S33) than the pro-*cis* open quadrant for its *cis* counterpart (174°, Fig. S22) (Table 3). Importantly, the peculiar geometry of *trans*-B_2A_1-^{3}MC allows for a second open quadrant (141°), which we alluded to earlier for the corresponding van der Waals adduct. *Cis* and *trans* ^{3}PESs from NEB calculations display similar energy profiles, although once again the two isomers can be expected to have different labilisation abilities, different solvation spheres and ion pairing capacities.[142] Once the *cis*/*trans*-B_2A_1-^{3}MC state is reached, intersystem crossing occurs to the singlet pentacoordinate *cis*/*trans*-B_2A_1-GS electrophilic species (Fig. S7 and S12), which are finally trapped with solvent to form the *cis*/*trans*-B_2A_2-GS final photoproducts (Fig. S35 and S40) lying 17 (*cis*) and 29 (*trans*) kcal/mol higher in energy than the reference.

2.5 Mixing between the *cis* and *trans* pathways

Up until this point we have, for reasons of simplicity, treated the *cis* and *trans* photoproduct formation pathways independently, but several interconnections can be envisaged. Very early in the process, in the B_3-^{3}MC region, we note that the two conformers pro-*cis*-$^3MC_{cis}$ and pro-*trans*-$^3MC_{cis}$ are nearly degenerate. The whole B_3-^{3}MC region is in fact a vast basin displaying a collection of local minima, between which interconversion is practically barrierless. The system can therefore certainly visit all these microstates. As soon as one bpy ligand is half decoordinated, the pentacoordinate κ^1-B_3 ground state *trans* species could convert to the *cis* one for an energy barrier of 13 kcal/mol (Fig. S60). As these electrophilic species are expected to undergo rapid quenching by coordinating solvent, this *trans-cis* conversion is probably not competitive. Later in the process, the B_2A_1 pentacoordinate ground state *trans* species could also convert to the *cis* one, this time for an energy barrier of 7 kcal/mol (Fig. S61), but again, this will be in competition with quenching by NCMe coordination. The B_2A_1-^{3}MC states, on the other hand, are almost degenerate and should be able to interconvert at almost no cost (barrierless process, calculated $\Delta E < 3$ kcal/mol) (Fig. S62).

3 Direct solvent coordination to triplet states : possible one-photon processes?

In addition to mechanisms implying the sequential absorption of two photons and going through an intermediate photoproduct ('stepwise' viewpoint), one-photon processes with binding of NCMe in the triplet state and direct formation of final photoproduct can also be envisaged ('concerted' viewpoint). Ordinarily under Wigner's rules solvent coordination to a pentacoordinate ^{3}MC state would be considered to be highly inefficient due to there being no metallic unoccupied acceptor orbital of the correct symmetry. However, we have recently postulated that electrostatic repulsion between an approaching ligand lone-pair and the unpaired metallic electron of a ^{3}MC state could result in switching the ordering of metal based orbitals and relocalising the unpaired electron with generation of a triplet state of alternative character.[113] This would therefore vacate the orbital originally accommodating the unpaired electron, thus enabling the solvent ligand to coordinate. We have previously hinted at the solvent accessibility of MC states and now explicitly address it.

3.1 Solvent coordination to B_3-MC and B_2A_1-MC states

From the B_3-^{3}MC region, direct coordination of acetonitrile onto a B_3-^{3}MC state could populate the κ^1-B_3A_1-^{3}MLCT state (calculated energy barriers being 18 kcal/mol in the *trans* case, Fig S57[113] and 14 kcal/mol in the *cis* case, Fig S50). Alternatively, the κ^1-B_3A_1-^{3}MLCT states could be circumvented entirely through direct and concerted solvent coordination and conversion from B_3-MC states to the B_2A_1-^{3}MC+B van der Waals adducts. Indeed, significantly smaller energy barriers are encountered for these latter processes, being 8 kcal/mol for both isomers (Fig. S51 and S58). These barriers are moderate enough so that we can consider these one-photon processes to be feasible and may be operative, at least in competition with reverse intersystem crossing to the singlet manifold, and in line with the lack of systematic evidence for κ^1-B_3A_1-GS primary photoproducts in some photolysis experiments.[89,124,125]

Further along the mechanism, we note that the B_3A_1-^{3}MLCT and B_2A_1-^{3}MC states are almost isoenergetic, and their direct connection is not excluded (direct population of the B_2A_1-^{3}MC state from a higher-lying ^{3}MLCT state is not excluded either). In this view, the van der Waals B_2A_1+B-^{3}MC states can be seen as traps to the desired reactivity through their neighbouring MECPs, which open a singlet state deactivation cascade to B_2A_1+B-GS and eventually κ^1-B_3A_1-GS.

The minimum energy path topologies of the *cis* and *trans* ^{3}PESs are shown in Figure 4. Note that two *cis* B_2A_2-^{3}MC states were identified as true minima, the one displaying elongated bonds towards the two bpy ligands (prefixed 'B+B', Fig. S26) being 5 kcal/mol higher in energy than the one displaying elongated bonds towards one acetonitrile and one bipyridine (prefixed 'A+B', Fig. S24). Barriers for their population from *cis*-B_2A_1-^{3}MC are 6 and 3 kcal/mol, respectively. In the *trans* series, one B_2A_2-^{3}MC minimum was optimised displaying elongations towards both bpy ligands (Fig. S35). The barrier for its population from *trans*-B_2A_1-^{3}MC is 7 kcal/mol. B_2A_2-^{3}MLCT states were also optimised although they do not take part in the formation of the bis(solvento) products (Fig. S27 and S36). Table 4 summarises their main geometrical parameters and Figure 4 presents the triplet energy profiles. The overall energy profiles are much flatter than in the singlet state however they are also uphill processes, in line with the poor photoreactivity of $[Ru(bpy)_3]^{2+}$ in MeCN. As in the singlet state, the *cis* ^{3}PES is lower in energy than the *trans* ^{3}PES by a few kcal/mol.

3.2 Second solvent coordination to ^{3}MC state van der Waals adducts : bypassing the B_2A_1 region

One could argue that B_2A_1 species are artificially brought in by our computational model and have little probability of existence in coordinating solvent. To probe this idea we have conducted NEB calculations bypassing the B_2A_1 region, *i.e.* connecting directly the van der Waals adducts B_2A_1+B to the final B_2A_2 region. In such calculations removal of bpy and approach of NCMe are concomitant. Representative examples are presented in Figures S52 (bottom) and S63 (bottom), showing that diffusion of bpy is the prerequisite to the formation of a van der Waals adduct between a pentacoordinate metal centre and the incoming acetonitrile molecule. This process involves barriers between 11-13 kcal/mol, values that correspond well to the energy gaps found between the B_2A_1+B and corresponding B_2A_1 species. Once the incoming NCMe is within van der Waals distance, a smaller barrier is encountered to populate the B_2A_2 triplet state (3-4 kcal/mol). Again these values are in very good agreement with the values found for the model reactions approaching NCMe onto a pentacoordinate B_2A_1 triplet state, presented in Figures S52 (top) and S63 (top). The fact that initial barriers for bpy diffusion and final barriers for NCMe coordination are perfectly consistent with the barriers involving the model B_2A_1 species indicates

that it seems an acceptable model to consider bpy diffusion prior to NCMe approach and coordination.

3.3 Mixing the *cis* and *trans* pathways

Here we return to possible *cis-trans* conversions, which we had previously envisaged for earlier stages of the reaction. In the B_2A_1 region, the peculiar geometry of the *trans* isomer displaying two open quadrants allows us to propose two preferential ways of approach for NCMe, depending on which, the two acetonitrile ligands will end in a *cis* or *trans* configuration. Nudged elastic band calculations were conducted between *cis*/*trans*-B_2A_1-^{3}MC and *cis*/*trans*-B_2A_2-^{3}MC minima (Fig. S52-S53, S59, S63-S64).

Table 4 : Ru-N distances (Å) for B_2A_2 triplet minima.

	A+B-elongated *cis*-B_2A_2-^{3}MC	B+B-elongated *cis*-B_2A_2-^{3}MC	*cis*-B_2A_2 ^{3}MLCT	*trans*-B_2A_2 ^{3}MC	*trans*-B_2A_2 ^{3}MLCT
Ru-N1	2.074	2.381	2.056	2.120	2.057
Ru-N2	2.072	2.127	2.018	2.494	2.052
Ru-N3	2.315	2.143	2.047	2.531	2.119
Ru-N4	2.153	2.461	2.094	2.121	2.121
Ru-$NCMe_a$	2.693	2.044	2.047	2.040	2.019
Ru-$NCMe_b$	2.048	2.042	2.065	2.038	2.023

Figure 4: Triplet state minima and minimum energy paths along the *cis* (top) and *trans* (bottom) pathway.

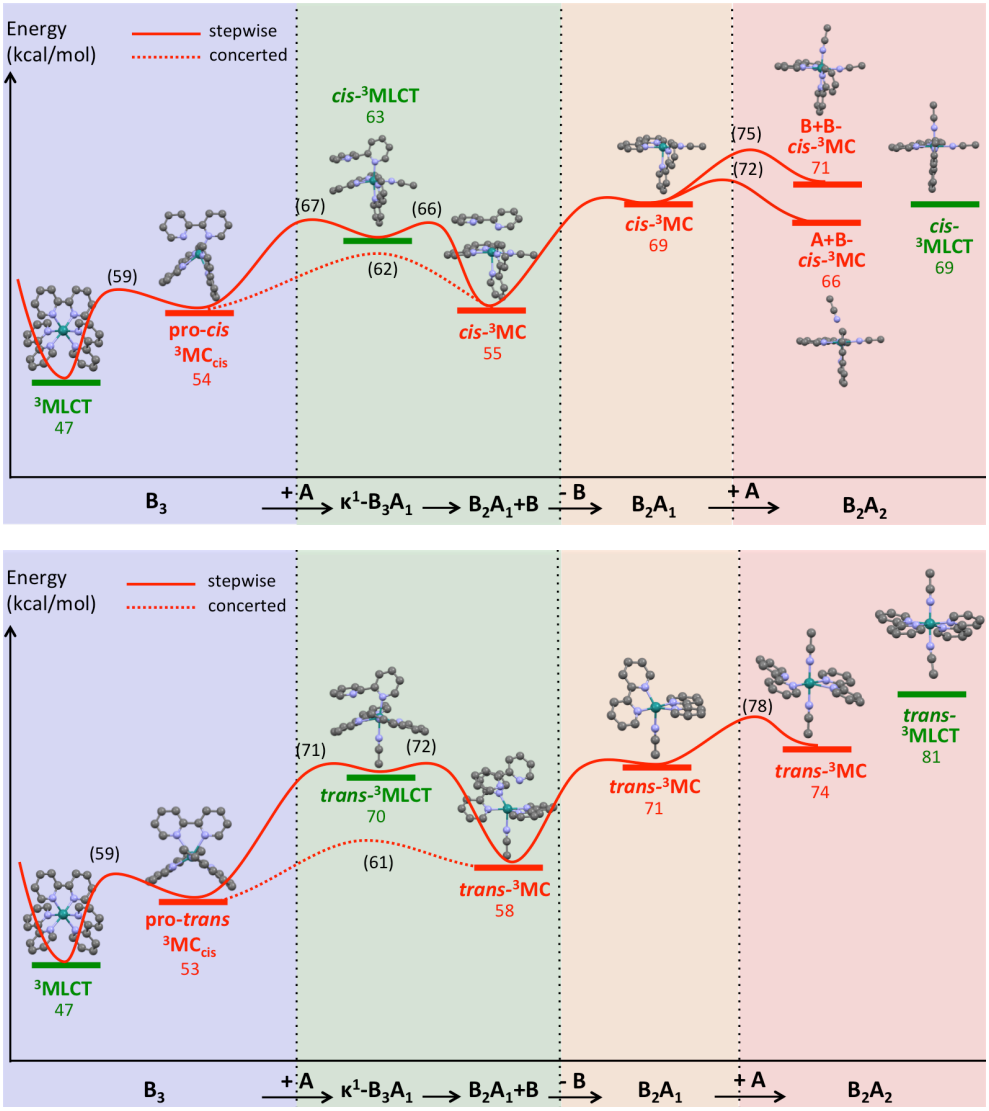

Most interestingly, the energy barriers for the *cis* → *cis* and *trans* → *cis* conversions are very small (3-5 kcal/mol), and smaller than that for the *trans* → *trans* conversion, for which the energy barrier to populate the *trans*-B_2A_2-^{3}MC state is 7 kcal/mol (Figure 5). It is also worth noting that the population of the lowest of all B_2A_2-^{3}MC states involves, from the corresponding adducts in which the incoming NCMe is within van der Waals distance (minima in the grey-shaded regions in Figure 5), similarly small energy barriers of 5 kcal/mol. In the B_2A_2 region the lowest

triplet state is of *cis* configuration, which possibly also contributes to favouring the formation of the *cis*-B_2A_2 final photoproduct from either the preceding *cis* or *trans*-B_2A_1-^{3}MC states.

In this section we have explored the possibility of a one-photon mechanism for photorelease of a bpy ligand from $[Ru(bpy)_3]^{2+}$ in which solvent ligand coordination and bpy ligand release may occur as sequential processes within the triplet manifold and circumvent ground state κ^1-bpy solvento intermediates. To summarise this novel mechanism (Scheme 3), after initial photoexcitation to, and then depopulation of the resultant B_3-MLCT state a solvent molecule may coordinate to the pro-*cis*- or pro-*trans*-B_3-MC_{cis} state to yield the van der Waals adducts *cis*- and *trans*-B_2A_1-MC+B respectively. Diffusion of the departing bpy ligand may then either be followed by intersystem crossing to the singlet state with a second solvent coordination, or solvent coordination to the B_2A_1-^{3}MC states and subsequent relaxation, to form the final B_2A_2-GS product. These final steps favour, both energetically and sterically, convergence of the preceding *cis*- and *trans*-pathways to formation the *cis*-B_2A_2 photoproduct.

4 Translation to, and significance for other photochemically reactive systems

In carrying out our detailed survey of the singlet and triplet potential energy surfaces associated with photochemical chelate ligand release and solvation of the archetypal complex $[Ru(bpy)_3]^{2+}$ we have attempted to establish a generalised mechanistic road map for excited state evolution during photoproduct formation for the wider family of tris(bidentate) complexes to which it belongs. This road map must necessarily encompass all key ground and excited state species that may play roles in the formation of photoproducts. Further it must also detail routes that select the formation of either *trans* bis(solvento) photoproducts or their more commonly encountered *cis* counterparts. Therefore in our calculations we have sought to probe the potential energy surfaces for the formation of both *cis*- and *trans*-$[Ru(bpy)_2(NCMe)_2]^{2+}$ through *cis*- and *trans*-$[Ru(bpy)_2(\kappa^1\text{-bpy})(NCMe)]^{2+}$ intermediates. Clearly, comparable excited state geometries will be accessible and involved in the photochemical processes of other complexes of this class that display far more efficient photochemistry.

Chelate ligand release might be anticipated to occur via one of several mechanistic scenarios; i) thermal ligand dechelation followed by thermal ligand dissociation, ii) photochemical ligand

dechelation followed by thermal ligand dissociation in the ground state, iii) photochemical ligand dechelation to yield a ground state intermediate with absorption of a second photon in a second photochemical ligand release step, and most intriguingly, iv) a single photon excitation process in which both dechelation and ligand release occur as sequential excited state events within the triplet manifold before finally forming closed shell ground state photoproducts. As is evident from the calculations presented here mechanism i) for the highly kinetically inert $[Ru(bpy)_3]^{2+}$ can be easily ruled out as activation barriers for the key processes would be prohibitively high. Similarly, mechanism ii) would be unlikely as thermal barriers for ligand dissociation from a $[Ru(bpy)_2(\kappa^1\text{-bpy})(solvent)]^{2+}$ type intermediate would be similarly prohibitive. However, we note that after photochemical initiation this may be feasible in cases with an extremely sterically encumbered ligand. We must therefore move on to mechanisms iii) and iv).

Mechanism iii) involving two sequential photochemical reactions implies the formation of a ground state ligand-loss intermediate bearing a κ^1-N^N ligand. In studies of the photochemistry of $[Ru(bpy)_3]^{2+}$ in hot acidic solutions in the presence of coordinating anions such as thiocyanate, non-isosbestic behaviour in UV-visible absorption spectroscopy indicate the formation of an intermediate, which one could presume to be of the form $[Ru(bpy)_2(\kappa^1\text{-bpy})(NCS)]^+$.[49,50] During the photolysis of the complex $[Ru(bpy)_2(3,3'\text{-dmbpy})]^{2+}$ (3,3'-dmbpy = 3,3'-dimethyl-2,2'-bipyridyl, Figure 6) with monitoring by ^{1}H NMR spectroscopy, two weak singlet resonances are observed ascribed to the now inequivalent 3,3'-dmbpy methyl groups of the solvento intermediate $[Ru(bpy)_2(\kappa^1\text{-}3,3'\text{-dmbpy})(NCMe)]^{2+}$.[102] Here, steric strain imparted by the 3-position methyl groups of the dmbpy ligand results in the complex being spring-loaded towards dechelation and thereby hindering rechelation, favouring formation of an observable monodentate intermediate. In recent work reported by Bonnet, photolysis of bis(thiomethyl)propane (bthmp) containing complexes, e.g. $[Ru(bpy)_2(bthmp)]^{2+}$ (Figure 6), reveals rapid photochemical conversion to ligand loss intermediates $[Ru(bpy)_2(\kappa^1\text{-bthmp})(solvent)]^{2+}$ followed by a much slower photochemical release of the monodentate bthmp ligand.[95] The high degree of conformational flexibility of the bthmp ligand may favour formation of the ground state intermediate solvent complex. The much slower nature of the second step likely stems from photochemical solvent ligand exchange processes that are more favourable than photochemical bthmp ligand release in the $[Ru(bpy)_2(\kappa^1\text{-bthmp})(solvent)]^{2+}$ intermediate. Similarly, the complex $[Ru(bpy)(btz)_2]^{2+}$, which favours *trans*

photoproduct formation, first rapidly and quantitatively forms the intermediate *trans*-[Ru(bpy)(κ^2-btz)(κ^1-btz)(NCMe)]$^{2+}$, with final photochemical loss of the κ^1-btz ligand being slow.[110] Due to the *trans* arrangement of the monodentate btz and acetonitrile ligands, the ^{3}MC state responsible for elongation of the Ru-N bond to the former will also elongate the corresponding bond to the latter. It would be expected that loss of the acetonitrile would be favoured over loss of btz, thus again resulting in photochemical solvent exchange to be the dominant process thereby enabling the reported observation, and indeed isolation of this κ^1-btz intermediate.[110]

Figure 5: Minimum energy paths for *cis-cis* (purple), *trans-trans* (orange) and *trans-cis* (blue and red) connections for the coordination of the second acetonitrile ligand onto pentacoordinate B_2A_1 ^{3}MC states. The grey-shaded regions correspond to regions of van der Waals adducts with the incoming NCMe (energy plateau or slight decrease). Arrows near the *trans*-B_2A_1 structure represent NCMe approaching in either open quadrant, leading to *trans* (orange arrow) or *cis* (blue or red arrows) products. Energies are given in kcal/mol with respect to the reference.

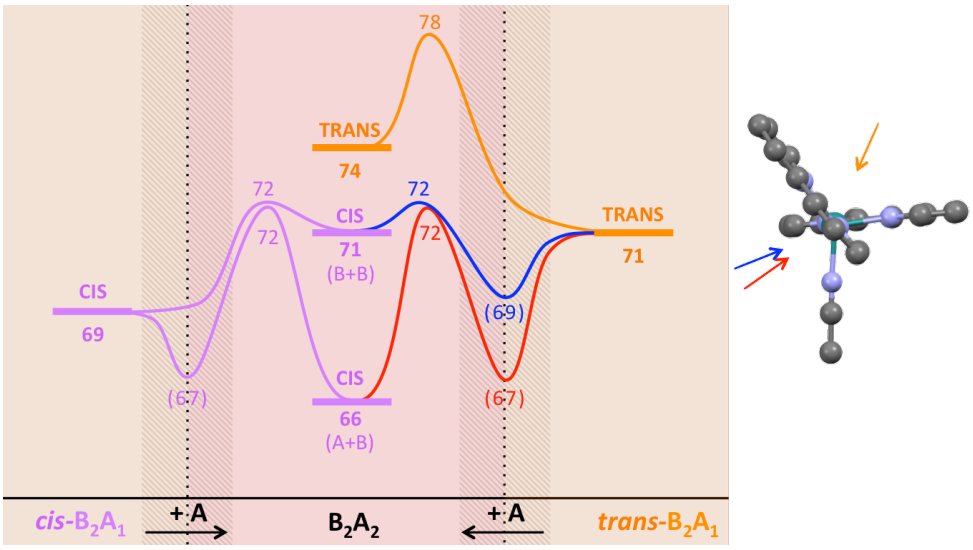

Scheme 3. Proposed multistep mechanism for a 1-photon process towards *cis*-$[Ru(bpy)_2(NCMe)_2]^{2+}$, with ligand dechelation and release occurring in the triplet state.

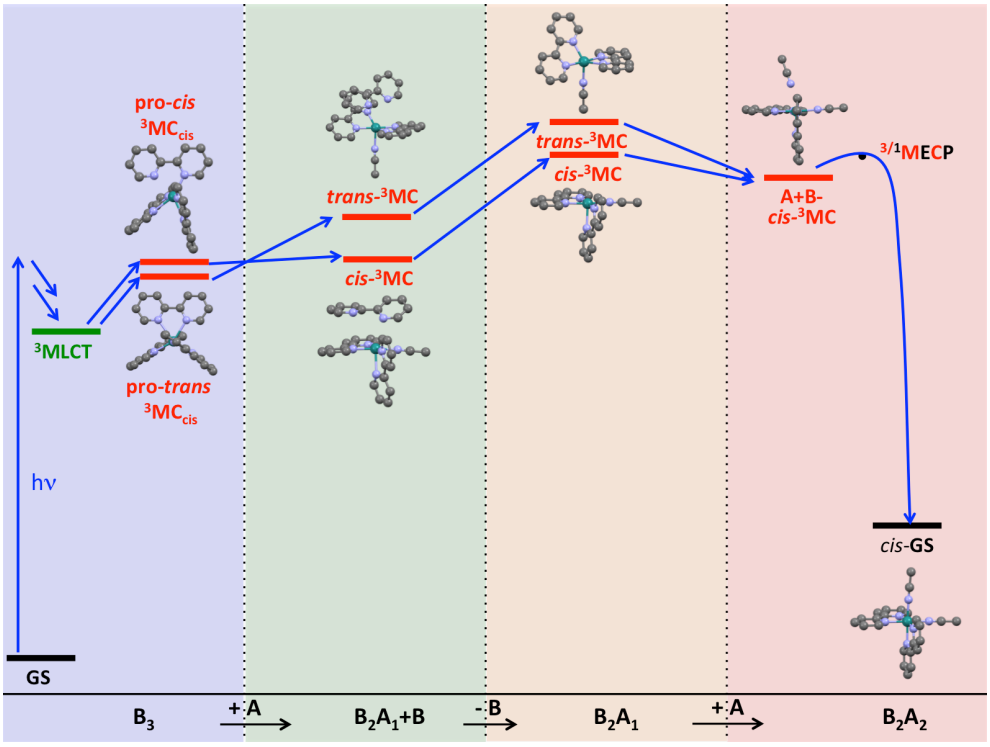

Finally, we come to the selection of either ground state κ^1-intermediates versus 'concerted' ligand coordination to triplet states and thus mechanism iv). In the examples outlined above it is likely spring-loaded dechelation (3,3'-dmbpy), conformational freedom of the departing ligand (bthmp) or a favourability for coplanarisation of the retained chelate ligands (bpy and btz) that favours formation of ground state closed shell intermediate photoproducts and thus operation of the two-step/two-photon mechanism (iii) for these complexes. Ligand-loss intermediate photoproducts are, however, relatively rarely observed and identified for tris(diimine) $[Ru(N\text{^}N)_3]^{2+}$-type complexes with more conformationally restricted ligands. For example, the bis(bpy) complexes $[Ru(bpy)_2(6,6'\text{-dmbpy})]^{2+}$ (6,6'-dmbpy = 6,6'-dimethyl-2,2'-bipyridyl)[89] and $[Ru(bpy)_2(btz)]^{2+}$ [110] rapidly eject the 6,6'-dmbpy and btz ligands respectively upon irradiation with clearly isosbestic UV-visible absorption spectra recorded during photolysis and no evidence of intermediates when monitored by NMR spectroscopy.

Figure 6. Structures of selected photochemically reactive ruthenium(II) bis-bpy complexes.

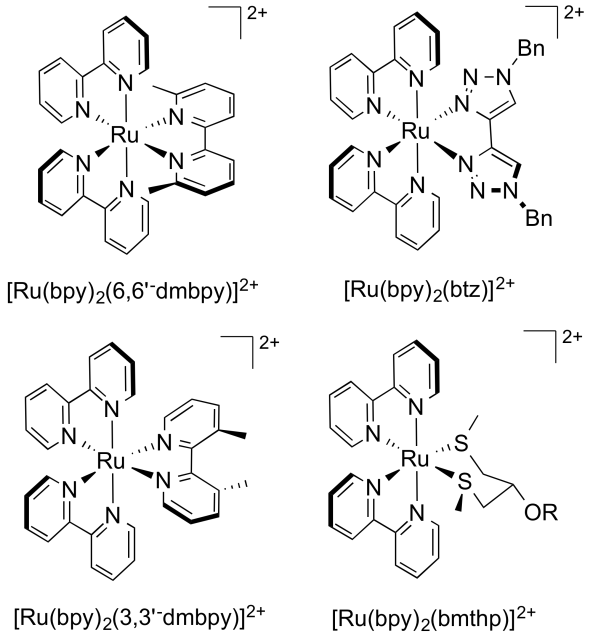

If solvent complexes were to be formed as ground state intermediate photoproducts one would reasonably expect that photochemical solvent exchange should effectively compete with, and even dominate over photochemical loss of the monodentate N^N ligand such that an intermediate should build up and be observable, even if at low concentrations. That no ligand loss intermediate is observed in many cases despite rapid and efficient photochemical consumption of the starting material may suggest that these intermediates may not in fact form at all in these systems. In our calculations we have shown that it is energetically feasible for acetonitrile to coordinate to B_3-^{3}MC species to form B_2A_1-^{3}MC+B van der Waals adducts in which the departing bpy ligand can already be said to be "on its way". We have also shown that a second solvent ligand may also be coordinated to the subsequent B_2A_1-^{3}MC states and access the B_2A_2 triplet region. Thus, through either intersystem crossing to the singlet state in the B_2A_1 region followed by solvent coordination, or the sequential coordination of two solvent ligands to triplet states followed by intersystem crossing to the singlet ground state in the B_2A_2 region, we show that it is entirely possible for ruthenium(II) tris(diimine) complexes (for example, $[Ru(bpy)_2(6,6'\text{-dmbpy})]^{2+}$ and $[Ru(bpy)_2(btz)]^{2+}$) to form the final photoproducts after absorption of a single photon and bypass formation of ground state κ^1 intermediate photoproducts entirely.

As highlighted earlier, photochemical ligand release from $Ru(bpy)_2$-based complexes tends to produce photoproducts with *cis* stereochemistry. $Ru(bpy)_2$-based complexes with two monodentate ligands in a *trans* arrangement are known, however, and have been crystallographically characterised.[143] In agreement with our calculations the two bpy ligands in these *trans* complexes deviate significantly from coplanarity due to a steric clash between the 6-position protons of the pyridine rings of the two ligands. This is therefore the likely reason for the relative dearth of ligand release $Ru(bpy)_2$-based photoproducts exhibiting *trans* stereochemistry. Our calculations further reveal that the key van der Waals adduct *trans*-B_2A_1-^{3}MC+B and the pentacoordinate ^{3}MC state *trans*-B_2A_1-^{3}MC in fact exhibit a hybrid structure partway between *trans* and *cis* stereochemistry, which relieves this steric strain. With access to the pro-*trans* quadrant of this ^{3}MC state being hindered by the departing bpy ligand this would therefore seem to favour solvent coordination at the second open quadrant, therefore driving the complex towards formation of the *cis* bis-acetonitrile product. Thus, whilst both the pro-*trans* and pro-*cis* excited state pathways are accessible through the B_3, B_3A_1, B_2A_1+B and B_2A_1 regions, these appear to converge to favour *cis*-B_2A_2, a configuration which, in addition, provides thermodynamically more stable final products. As such intermediate excited state species will be relevant to a large number of other photoreactive bis-bpy complexes this accounts for the predominance of photoproducts of *cis* stereochemistry.

Conversely, for the heteroleptic complex $[Ru(bpy)(btz)_2]^{2+}$ no such steric clash exists between the bpy and btz ligands when they become coplanar in *trans*-$[Ru(bpy)(\kappa^2\text{-btz})(\kappa^1\text{-btz})(NCMe)]^{2+}$ and *trans*-$[Ru(bpy)(btz)(NCMe)_2]^{2+}$. One would therefore not expect the appearance of hybrid van der Waals adduct and pentacoordinate ^{3}MC states comparable to *trans*-B_2A_1-MC+B (indeed, one would expect the bpy and btz to remain coplanar as in the cyrstallographically characterised κ^1-btz intermediate),[110] and thus little driving force to switch from *trans* to *cis* photoproduct formation pathways. Calculations on the *cis* and *trans* isomers of the final photoproducts showed the *latter* to be the most stable.[105] Therefore it seems likely that the relative energy ordering of the comparable *cis* and *trans* pathways for $[Ru(bpy)_2(btz)]^{2+}$ is inverted compared to $[Ru(bpy)_3]^{2+}$.

The nature of both the departing and retained spectator ligands present, as well as the nature of the incoming solvent (or coordinating anions) are therefore crucial for the selection of the preference for *cis* versus *trans* photoproduct formation but also the favourability of the formation of

singlet ground state intermediate photoproducts and thus the operation of a two photon (iii) or single photon triplet state solvation (iv) mechanism. For some complexes it will also be possible that both mechanisms are simultaneously operative.

For $[Ru(bpy)_3]^{2+}$ the energy landscape associated with formation of acetonitrile-containing photoproducts involves an uphill climb through the triplet manifold and accounts for the low photochemical reactivity displayed by the complex. For the highly photochemically reactive $[Ru(bpy)_2(6,6'\text{-dmbpy})]^{2+}$ it is proposed that the steric congestion imparted by the 6'6'-dmbpy methyl group weakens the Ru-N bonds and thus stabilises the ^{3}MC states relative to the ^{3}MLCT state. This then makes the depopulation of the ^{3}MLCT states and initiation of photochemical reactivity far easier than for $[Ru(bpy)_3]^{2+}$. However, it can also be said that the steric strain will also *de*stabilise the ground and ^{3}MLCT states relative to ^{3}MC states in which the strain is intrinsically relieved due to the occurrence of elongated metal-ligand bonds. As the energy profiles for the photoreaction mechanism are necessarily related to the reference of the energy of the ground state this should result in a flattening of the overall excited state minimum energy paths with respect to the starting ^{3}MLCT state. This would result in making states along this path inherently more accessible and therefore photochemical reactivity far more efficient. For $[Ru(bpy)_2(btz)]^{2+}$ a similar result can be envisaged through a different cause : the destabilisation of the ^{3}MLCT state with respect to that of $[Ru(bpy)_3]^{2+}$ would again result in far more facile access to excited state PES photoproductive pathways. In order to verify these inferences we are currently using the generalised road map derived in this work to chart and explore the analogous ground and excited state potential energy landscapes for photoproduct formation in these and other photolabile systems. Explicit solvation would also improve modelling by comparison to the current bimolecular reaction model, which in itself is a challenging prospect. Results from these on-going studies will be reported elsewhere in due course.

Conclusions

Ligand photorelease is a very active field of research in relation to photoactivated chemotherapy (PACT) or photorelease of biologically active molecules. From the point of view of fundamental inorganic photochemistry, the microscopic mechanisms underpinning multistep ligand photoex-

change processes have been unclear and have still required thorough investigation. The theoretical study reported herein has allowed us to establish all the elementary steps of a dissociative ligand photoexchange mechanism on a model reaction involving $[Ru(bpy)_3]^{2+}$ as reactant and acetonitrile as the incoming ligand. This has enabled us to highlight two main mechanisms involving either two sequential photochemical processes or a single process after absorption of just one photon. The former involves stepwise bpy dissociation through the formation of κ^1 intermediate photoproducts incorporating one NCMe ligand and absorption of a second photon that opens the way to the photorelease of the κ^1-bpy ligand, followed by the coordination of a second NCMe ligand. In the latter case, following absorption of just one photon the ligand dechelation, dissociation and solvent coordination may all happen as a set of sequential steps *all occurring in the triplet excited state*. Both *cis* and *trans* products could be formed in either mechanism, with energy barriers of similar magnitude. The *trans* pathway is generally slightly higher in energy than the *cis* pathway for the model $[Ru(bpy)_3]^{2+}$ system, except in a few regions where both are almost isoenergetic and may communicate at little cost. Associative mechanisms have been occasionally proposed in Ru(II),[90] Rh(I),[144] and Re(I)[145] photochemistry and it is important to note that several mechanisms could be operative, as exemplified by the complex photochemistry of $Fe(CO)_5$.[146,147,148,141,149] Experimental conditions necessarily have a tremendous impact on the outcome of a photochemical reaction.[150] In this respect, ligand photoexchange experiments performed under pulsed excitation could bring a wealth of mechanistic insights. We hope this theoretical study will stimulate further experimental studies that would feed the discussion in this exciting field of research. We also hope that these results provide a transferable road map that can be translated to other systems where both departing and 'spectator' ligand influence the selection of whether stepwise/two-photon or concerted/one-photon mechanisms are operative and the selection of product stereochemistry. Further, we hope that this will offer insights that aid the development in the molecular design of efficient photoreactive complexes for PACT and as photomechanical molecular machines.

ASSOCIATED CONTENT

Supporting Information

Computational details, structures, energies and selected orbitals of all minima and minimum energy crossing points, plots of minimum energy paths, and TDDFT calculations (pdf); Cartesian coordinates of all minima and MECPs (zip).

The Supporting Information is available free of charge on the ACS Publications website.

AUTHOR INFORMATION

Corresponding Authors

* P.I.Elliott@hud.ac.uk

* isabelle.dixon@irsamc.ups-tlse.fr

Author Contributions

The manuscript was written through contributions of all authors.

Funding Sources

No competing financial interests have been declared.

Acknowledgements

We thank the French Ministry for Higher Education and Research for a Ph. D. fellowship to AS. HPC resources from LCPQ and from CALMIP (p18013 project) are gratefully acknowledged. PE also thanks the University of Huddersfield for support and the 3M Business and Innovation Centre for additional HPC resources.

References

(1) Adamson, A. W.; Demas, J. N. A New Photosensitizer. Tris(2,2'-Bipyridine)Ruthenium(II) Chloride. *J. Am. Chem. Soc.* **1971**, *93*, 1800–1801. https://doi.org/10.1021/ja00736a049.

(2) Gafney, H. D.; Adamson, A. W. Excited State $Ru(Bipyr)_3^{2+}$ as an Electron-Transfer Reductant. *J. Am. Chem. Soc.* **1972**, *94*, 8238–8239. https://doi.org/10.1021/ja00778a054.

(3) Crosby, G. A.; Watts, R. J. Spectroscopic Characterization of Complexes of Ruthenium(II) and Iridium(III) with 4,4'-Diphenyl-2,2'-Bipyridine and 4,7-Diphenyl-1,10-Phenanthroline. *J. Am. Chem. Soc.* **1971**, *93*, 3184–3188. https://doi.org/10.1021/ja00742a016.

(4) Demas, J. N.; Crosby, G. A. Quantum Efficiencies on Transition Metal Complexes. II. Charge-Transfer Luminescence. *J. Am. Chem. Soc.* **1971**, *93*, 2841–2847. https://doi.org/10.1021/ja00741a003.

(5) Harrigan, R. W.; Hager, G. D.; Crosby, G. A. Evidence for Multiple-State Emission from Ruthenium(II) Complexes. *Chem. Phys. Lett.* **1973**, *21*, 487–490. https://doi.org/10.1016/0009-2614(73)80290-8.

(6) Hager, G. D.; Crosby, G. A. Charge-Transfer Excited States of Ruthenium(II) Complexes. I. Quantum Yield and Decay Measurements. *J. Am. Chem. Soc.* **1975**, *97*, 7031–7037. https://doi.org/10.1021/ja00857a013.

(7) Crosby, G. A. Spectroscopic Investigations of Excited States of Transition-Metal Complexes. *Acc. Chem. Res.* **1975**, *8*, 231–238. https://doi.org/10.1021/ar50091a003.

(8) Demas, J. N.; Diemente, D.; Harris, E. W. Oxygen Quenching of Charge-Transfer Excited States of Ruthenium(II) Complexes. Evidence for Singlet Oxygen Production. *J. Am. Chem. Soc.* **1973**, *95*, 6864–6865. https://doi.org/10.1021/ja00801a073.

(9) Demas, J. N.; Addington, J. W. Luminescence Quenching of the Tris(2,2'-Bipyridine)Ruthenium(II) and Tris(1,10-Phenanthroline)Ruthenium(II) Cations. *J. Am. Chem. Soc.* **1976**, *98*, 5800–5806. https://doi.org/10.1021/ja00435a010.

(10) Demas, J. N.; Harris, E. W.; McBride, R. P. Energy Transfer from Luminescent Transition Metal Complexes to Oxygen. *J. Am. Chem. Soc.* **1977**, *99*, 3547–3551. https://doi.org/10.1021/ja00453a001.

(11) Natarajan, P.; Endicott, J. F. Intermediates Generated in the Charge Transfer to Ligand Photochemistry of Ruthenium(II) Pyridine and Bipyridyl Complexes. *J. Am. Chem. Soc.* **1972**, *94*, 5909–5910. https://doi.org/10.1021/ja00771a070.

(12) Natarajan, P.; Endicott, J. F. Direct Observation of the Dibromide Radical Anion Oxidation of Tris(Bipyridyl)Ruthenium(II). Evidence for a Triplet-to-Triplet Energy Transfer Mechanism in the Photosensitized Redox Decomposition of Cobalt(III) Substrates. *J. Phys. Chem.* **1973**, *77*, 971–972. https://doi.org/10.1021/j100626a025.

(13) Wrighton, M.; Markham, J. Quenching of the Luminescent State of Tris(2,2'-Bipyridine)Ruthenium(II) by Electronic Energy Transfer. *J. Phys. Chem.* **1973**, *77*, 3042–3044. https://doi.org/10.1021/j100644a002.

(14) Bock, C. R.; Meyer, T. J.; Whitten, D. G. Electron Transfer Quenching of the Luminescent Excited State of Tris(2,2'-Bipyridine)Ruthenium(II). Flash Photolysis Relaxation Technique for Measuring the Rates of Very Rapid Electron Transfer Reactions. *J. Am. Chem. Soc.* **1974**, *96*, 4710–4712. https://doi.org/10.1021/ja00821a078.

(15) Young, R. C.; Meyer, T. J.; Whitten, D. G. Electron Transfer Quenching of Excited States of Metal Complexes. *J. Am. Chem. Soc.* **1976**, *98*, 286–287. https://doi.org/10.1021/ja00417a073.

(16) Van Houten, J.; Watts, R. J. Effect of Ligand and Solvent Deuteration on the Excited State Properties of the Tris(2,2'-Bipyridyl)Ruthenium(II) Ion in Aqueous Solution. Evidence for Electron Transfer to Solvent. *J. Am. Chem. Soc.* **1975**, *97*, 3843–3844. https://doi.org/10.1021/ja00846a062.

(17) Navon, G.; Sutin, N. Mechanism of the Quenching of the Phosphorescence of Tris(2,2'-Bipyridine)Ruthenium(II) by Some Cobalt(III) and Ruthenium(III) Complexes. *Inorg. Chem.* **1974**, *13*, 2159–2164. https://doi.org/10.1021/ic50139a021.

(18) Lin, C.-T.; Böttcher, W.; Chou, M.; Creutz, C.; Sutin, N. Mechanism of the Quenching of the Emission of Substituted Polypyridineruthenium(II) Complexes by Iron(III), Chromium(III), and Europium(III) Ions. *J. Am. Chem. Soc.* **1976**, *98*, 6536–6544. https://doi.org/10.1021/ja00437a020.

(19) Creutz, C.; Sutin, N. Electron-Transfer Reactions of Excited States. Reductive Quenching of the Tris(2,2'-Bipyridine)Ruthenium(II) Luminescence. *Inorg. Chem.* **1976**, *15*, 496–499. https://doi.org/10.1021/ic50156a062.

(20) Creutz, C.; Sutin, N. Electron-Transfer Reactions of Excited States: Direct Evidence for Reduction of the Charge-Transfer Excited State of Tris(2,2'-Bipyridine)Ruthenium(II). *J. Am. Chem. Soc.* **1976**, *98*, 6384–6385. https://doi.org/10.1021/ja00436a054.

(21) Laurence, G. S.; Balzani, Vincenzo. Reduction by the Triplet Charge-Transfer State of Tris(Bipyridyl)Ruthenium(II). Photochemical Reaction between Tris(Bipyridyl) Ruthenium(II) and Thallium(III). *Inorg. Chem.* **1974**, *13*, 2976–2982. https://doi.org/10.1021/ic50142a039.

(22) Bolletta, F.; Maestri, M.; Moggi, L.; Balzani, V. Bimolecular Electron Transfer Reactions of Electronically Excited States of Coordination Compounds. *J. Chem. Soc. Chem. Commun.* **1975**, 901–902. https://doi.org/10.1039/C39750000901.

(23) Balzani, V.; Moggi, L.; Manfrin, M. F.; Bolletta, F.; Laurence, G. S. Quenching and Sensitization Processes of Coordination Compounds. *Coord. Chem. Rev.* **1975**, *15*, 321–433. https://doi.org/10.1016/S0010-8545(00)82070-6.

(24) Juris, A.; Gandolfi, M. T.; Manfrin, M. F.; Balzani, V. Electron and Energy Transfer Mechanisms in the Quenching of the Tris(2,2'-Bipyridine)Ruthenium(II) Luminescence by Cyanide Complexes. *J. Am. Chem. Soc.* **1976**, *98*, 1047–1048. https://doi.org/10.1021/ja00420a046.

(25) Meyer, T. J.; Sheridan, M. V.; Sherman, B. D. Mechanisms of Molecular Water Oxidation in Solution and on Oxide Surfaces. *Chem. Soc. Rev.* **2017**, *46*, 6148–6169. https://doi.org/10.1039/C7CS00465F.

(26) Garrido-Barros, P.; Gimbert-Suriñach, C.; Matheu, R.; Sala, X.; Llobet, A. How to Make an Efficient and Robust Molecular Catalyst for Water Oxidation. *Chem. Soc. Rev.* **2017**, *46*, 6088–6098. https://doi.org/10.1039/C7CS00248C.

(27) Matheu, R.; Ertem, M. Z.; Gimbert-Suriñach, C.; Sala, X.; Llobet, A. Seven Coordinated Molecular Ruthenium–Water Oxidation Catalysts: A Coordination Chemistry Journey. *Chem. Rev.* **2019**, *119*, 3453–3471. https://doi.org/10.1021/acs.chemrev.8b00537.

(28) Pashaei, B.; Shahroosvand, H.; Graetzel, M.; Nazeeruddin, M. K. Influence of Ancillary Ligands in Dye-Sensitized Solar Cells. *Chem. Rev.* **2016**, *116*, 9485–9564. https://doi.org/10.1021/acs.chemrev.5b00621.

(29) Aghazada, S.; Nazeeruddin, M. K. Ruthenium Complexes as Sensitizers in Dye-Sensitized Solar Cells. *Inorganics* **2018**, *6*, 52. https://doi.org/10.3390/inorganics6020052.

(30) Prier, C. K.; Rankic, D. A.; MacMillan, D. W. C. Visible Light Photoredox Catalysis with Transition Metal Complexes: Applications in Organic Synthesis. *Chem. Rev.* **2013**, *113*, 5322–5363. https://doi.org/10.1021/cr300503r.

(31) Buzzetti, L.; Crisenza, G. E. M.; Melchiorre, P. Mechanistic Studies in Photocatalysis. *Angew. Chem. Int. Ed.* **2019**, *58*, 3730–3747. https://doi.org/10.1002/anie.201809984.

(32) Shum, J.; Leung, P. K.-K.; Lo, K. K.-W. Luminescent Ruthenium(II) Polypyridine Complexes for a Wide Variety of Biomolecular and Cellular Applications. *Inorg. Chem.* **2019**, *58*, 2231–2247. https://doi.org/10.1021/acs.inorgchem.8b02979.

(33) Balzani, V.; Juris, A.; Barigelletti, F.; Belser, P.; von Zelewsky, A. Photophysical Properties of Ruthenium(II) Polypyridine Complexes. *Riken Quaterly* **1984**, *78*, 78–85.

(34) Juris, A.; Balzani, V.; Barigelletti, F.; Campagna, S.; Belser, P.; von Zelewsky, A. Ru(II) Polypyridine Complexes : Photophysics, Photochemistry, Electrochemistry, and Chemiluminescence. *Coord. Chem. Rev.* **1988**, *84*, 85–277. https://doi.org/10.1016/0010-8545(88)80032-8.

(35) Lever, A. B. P. Electrochemical Parametrization of Metal Complex Redox Potentials, Using the Ruthenium(III)/Ruthenium(II) Couple to Generate a Ligand Electrochemical Series. *Inorg. Chem.* **1990**, *29*, 1271–1285. https://doi.org/10.1021/ic00331a030.

(36) Roundhill, D. M. *Photochemistry and Photophysics of Metal Complexes*; Modern Inorganic Chemistry; Springer, 1994. https://doi.org/10.1007/978-1-4899-1495-8.

(37) Campagna, S.; Puntoriero, F.; Nastasi, F.; Bergamini, G.; Balzani, V. Photochemistry and Photophysics of Coordination Compounds: Ruthenium. In *Photochemistry and Photophysics of Coordination Compounds I*; Balzani, V., Campagna, S., Eds.; Topics in Current Chemistry; Springer, 2007; Vol. 280, pp 117–214. https://doi.org/10.1007/128_2007_133.

(38) Limburg, B.; Bouwman, E.; Bonnet, S. Rate and Stability of Photocatalytic Water Oxidation Using $[Ru(Bpy)_3]^{2+}$ as Photosensitizer. *ACS Catal.* **2016**, *6*, 5273–5284. https://doi.org/10.1021/acscatal.6b00107.

(39) Chakraborty, S.; Edwards, E. H.; Kandemir, B.; Bren, K. L. Photochemical Hydrogen

Evolution from Neutral Water with a Cobalt Metallopeptide Catalyst. *Inorg. Chem.* **2019**, *58*, 16402–16410. https://doi.org/10.1021/acs.inorgchem.9b02067.

(40) Ford, P. C.; Stuermer, D. H.; McDonald, D. P. Photochemical Reaction Pathways of Pentaammineruthenium(II) Complexes. *J. Am. Chem. Soc.* **1969**, *91*, 6209–6211. https://doi.org/10.1021/ja01050a066.

(41) Ford, P. C.; Chaisson, D. A.; Stuermer, D. H. Quantum Yields for the Photoaquation Reactions of $[Ru(NH_3)_5(Py)]^{2+}$ and Related Complexes: An Unusual Dependence on Acid Concentration. *J. Chem. Soc. Chem. Commun.* **1971**, 530–531. https://doi.org/10.1039/C29710000530.

(42) Chaisson, D. A.; Hintze, R. E.; Stuermer, D. H.; Petersen, J. D.; McDonald, D. P.; Ford, P. C. Photochemical Reaction Pathways of Ruthenium(II) Complexes. III. Metal-to-Ligand Charge-Transfer Excitation of the Pentaamminepyridineruthenium(II) Cation and Related Species. *J. Am. Chem. Soc.* **1972**, *94*, 6665–6673. https://doi.org/10.1021/ja00774a017.

(43) Malouf, G.; Ford, P. C. Photochemical Reaction Pathways of Ruthenium(II) Complexes. Evidence Regarding the Reactive Excited State(s) from Metal-to-Ligand Charge Transfer Excitation of $Ru(NH_3)_5^{2+}$ and Related Complexes. *J. Am. Chem. Soc.* **1974**, *96*, 601–603. https://doi.org/10.1021/ja00809a056.

(44) Van Houten, J.; Watts, R. J. Temperature Dependence of the Photophysical and Photochemical Properties of the Tris(2,2'-Bipyridyl) Ruthenium(II) Ion in Aqueous Solution. *J. Am. Chem. Soc.* **1976**, *98*, 4853–4858. https://doi.org/10.1021/ja00432a028.

(45) Van Houten, J.; Watts, R. J. Photochemistry of Tris(2,2'-Bipyridyl)Ruthenium(II) in Aqueous Solution. *Inorg. Chem.* **1978**, *17*, 3381–3385. https://doi.org/10.1021/ic50190a016.

(46) Gleria, M.; Minto, F.; Beggiato, G.; Bortolus, P. Photochemistry of Tris(2,2'-Bipyridine)Ruthenium(II) in Chlorinated Solvents. *J. Chem. Soc. Chem. Commun.* **1978**, 285. https://doi.org/10.1039/C3978000285A.

(47) Hoggard, P. E.; Porter, G. B. Photoanation of the Tris(2,2'-Bipyridine) Ruthenium(II) Cation by Thiocyanate. *J. Am. Chem. Soc.* **1978**, *100*, 1457–1463. https://doi.org/10.1021/ja00473a021.

(48) Wallace, W. M.; Hoggard, P. E. A Simple Photochemical Synthesis of Some Bis(Bipyridyl)Ruthenium(II) Complexes. *Inorg. Chem.* **1979**, *18*, 2934–2935. https://doi.org/10.1021/ic50200a066.

(49) Durham, B.; Walsh, J. L.; Carter, C. L.; Meyer, T. J. Synthetic Applications of Photosubstitution Reactions of Poly(Pyridyl) Complexes of Ruthenium(II). *Inorg. Chem.* **1980**, *19*, 860–865. https://doi.org/10.1021/ic50206a014.

(50) Durham, B.; Caspar, J. V.; Nagle, J. K.; Meyer, T. J. Photochemistry of $Ru(Bpy)_3^{2+}$. *J. Am. Chem. Soc.* **1982**, *104*, 4803–4810. https://doi.org/10.1021/ja00382a012.

(51) Pinnick, D. V.; Durham, B. Photosubstitution Reactions of $Ru(Bpy)_2XY^{n+}$ Complexes. *Inorg. Chem.* **1984**, *23*, 1440–1445. https://doi.org/10.1021/ic00178a028.

(52) Allen, L. R.; Craft, P. P.; Durham, B.; Walsh, J. Substitution Reactions of Ruthenium(II) Complexes Containing 2,2'-Bipyridine and 1,10-Phenanthroline. *Inorg. Chem.* **1987**, *26*, 53–56. https://doi.org/10.1021/ic00248a012.

(53) Suen, H.-F.; Wilson, S. W.; Pomerantz, M.; Walsh, J. L. Photosubstitution Reactions of Terpyridine Complexes of Ruthenium(II). *Inorg. Chem.* **1989**, *28*, 786–791. https://doi.org/10.1021/ic00303a034.

(54) Hecker, C. R.; Fanwick, P. E.; McMillin, D. R. Evidence for Dissociative Photosubstitution Reactions of $[Ru(Trpy)(Bpy)(NCCH_3)]^{2+}$. Crystal and Molecular Structure of $[Ru(Trpy)(Bpy)(Py)](PF_6)_2.(CH_3)_2CO$. *Inorg. Chem.* **1991**, *30*, 659–666. https://doi.org/10.1021/ic00004a013.

(55) Bonnet, S.; Collin, J.-P. Ruthenium-Based Light-Driven Molecular Machine Prototypes: Synthesis and Properties. *Chem. Soc. Rev.* **2008**, *37*, 1207–1217. https://doi.org/10.1039/b713678c.

(56) Colasson, B.; Credi, A.; Ragazzon, G. Light-Driven Molecular Machines Based on Ruthenium(II) Polypyridine Complexes: Strategies and Recent Advances. *Coord. Chem. Rev.* **2016**, *325*, 125–134. https://doi.org/10.1016/j.ccr.2016.02.012.

(57) Ford, P. C. Metal Complex Strategies for Photo-Uncaging the Small Molecule Bioregulators Nitric Oxide and Carbon Monoxide. *Coord. Chem. Rev.* **2018**, *376*, 548–564. https://doi.org/10.1016/j.ccr.2018.07.018.

(58) White, J. K.; Schmehl, R. H.; Turro, C. An Overview of Photosubstitution Reactions of Ru(II) Imine Complexes and Their Application in Photobiology and Photodynamic Therapy. *Inorganica Chim. Acta* **2017**, *454*, 7–20. https://doi.org/10.1016/j.ica.2016.06.007.

(59) Li, A.; Turro, C.; Kodanko, J. J. Ru(II) Polypyridyl Complexes as Photocages for Bioactive Compounds Containing Nitriles and Aromatic Heterocycles. *Chem. Commun.* **2018**, *54*, 1280–1290. https://doi.org/10.1039/C7CC09000E.

(60) Li, A.; Turro, C.; Kodanko, J. J. Ru(II) Polypyridyl Complexes Derived from Tetradentate Ancillary Ligands for Effective Photocaging. *Acc. Chem. Res.* **2018**, *51*, 1415–1421. https://doi.org/10.1021/acs.accounts.8b00066.

(61) Bonnet, S. Why Develop Photoactivated Chemotherapy? *Dalton Trans.* **2018**, *47*, 10330–10343. https://doi.org/10.1039/C8DT01585F.

(62) Havrylyuk, D.; Stevens, K.; Parkin, S.; Glazer, E. C. Toward Optimal Ru(II) Photocages: Balancing Photochemistry, Stability, and Biocompatibility Through Fine Tuning of Steric, Electronic, and Physiochemical Features. *Inorg. Chem.* **2020**, *59*, 1006–1013. https://doi.org/10.1021/acs.inorgchem.9b02065.

(63) Toupin, N. P.; Nadella, S.; Steinke, S. J.; Turro, C.; Kodanko, J. J. Dual-Action Ru(II) Complexes with Bulky π-Expansive Ligands: Phototoxicity without DNA Intercalation. *Inorg. Chem.* **2020**, *59*, 3919–3933. https://doi.org/10.1021/acs.inorgchem.9b03585.

(64) Loftus, L. M.; Rack, J. J.; Turro, C. Photoinduced Ligand Dissociation Follows Reverse

Energy Gap Law: Nitrile Photodissociation from Low Energy ^{3}MLCT Excited States. *Chem. Commun.* **2020**, *56*, 4070–4073. https://doi.org/10.1039/C9CC10095D.

(65) Adamson, A. W. Photochemistry of Complex Ions. IV. Role of Quartet Excited States in the Photochemistry of Chromium(III) Complexes. *J. Phys. Chem.* **1967**, *71*, 798–808. https://doi.org/10.1021/j100863a003.

(66) Zink, J. I. Model for Predicting the Photoreactions and Relative Quantum Yields of Transition Metal and Organometallic Complexes. I. Chromium(III). *J. Am. Chem. Soc.* **1972**, *94*, 8039–8045. https://doi.org/10.1021/ja00778a018.

(67) Zink, J. I. Model for Predicting the Photoreactions and Relative Quantum Yields of Transition Metal and Organometallic Complexes. II. Cobalt(III) and Rhodium(III). *Inorg. Chem.* **1973**, *12*, 1018–1024. https://doi.org/10.1021/ic50123a010.

(68) Zink, J. I. Relative Ligand Labilization in Transition Metal Photochemistry. Molecular Orbital Approach. *J. Am. Chem. Soc.* **1974**, *96*, 4464–4470. https://doi.org/10.1021/ja00821a019.

(69) Wrighton, M.; Gray, H. B.; Hammond, G. S. A Model for the Substitutional Reactivity of Ligand Field Excited States. *Mol. Photochem.* **1973**, *5*, 165–178. https://doi.org/10.1002/chin.197338300.

(70) Vanquickenborne, L. G.; Ceulemans, A. On the Photochemical Substitution Reactions of Hexacoordinated Transition Metal Complexes. *J. Am. Chem. Soc.* **1977**, *99*, 2208–2214. https://doi.org/10.1021/ja00449a030.

(71) Vanquickenborne, L. G.; Ceulemans, A. Photostereochemistry and Electronic Selection Rules in Strong-Field d^6 Transition-Metal Complexes. *Inorg. Chem.* **1978**, *17*, 2730–2736. https://doi.org/10.1021/ic50188a009.

(72) Vanquickenborne, L. G.; Ceulemans, A. Photolabilization and Bond Indices in Hexacoordinated Transition-Metal Complexes: The D_{2h} Case. *Inorg. Chem.* **1981**, *20*, 110–113. https://doi.org/10.1021/ic50215a025.

(73) Daniel, C.; Gourlaouen, C. Chemical Bonding Alteration upon Electronic Excitation in Transition Metal Complexes. *Coord. Chem. Rev.* **2017**, *344*, 131–149. https://doi.org/10.1016/j.ccr.2016.10.010.

(74) Chergui, M.; Collet, E. Photoinduced Structural Dynamics of Molecular Systems Mapped by Time-Resolved X-Ray Methods. *Chem. Rev.* **2017**, *117*, 11025–11065. https://doi.org/10.1021/acs.chemrev.6b00831.

(75) Thompson, D. W.; Ito, A.; Meyer, T. J. $[Ru(Bpy)_3]^{2+*}$ and Other Remarkable Metal-to-Ligand Charge Transfer (MLCT) Excited States. *Pure Appl. Chem.* **2013**, *85*, 1257–1305. https://doi.org/10.1351/PAC-CON-13-03-04.

(76) Adamson, A. W.; Waltz, W. L.; Zinato, E.; Watts, D. W.; Fleischauer, P. D.; Lindholm, R. D. Photochemistry of Transition-Metal Coordination Compounds. *Chem. Rev.* **1968**, *68*, 541–585. https://doi.org/10.1021/cr60255a002.

(77) Endicott, J. F.; Ramasami, T.; Tamilarasan, R.; Lessard, R. B.; Ryu, C. K.; Brubaker, G. R. Structure and Reactivity of the Metal-Centered Transition Metal Excited States. *Coord. Chem. Rev.* **1987**, *77*, 1–87. https://doi.org/10.1016/0010-8545(87)85032-4.

(78) Caspar, J. V.; Meyer, T. J. Photochemistry of MLCT Excited States. Effect of Nonchromophoric Ligand Variations on Photophysical Properties in the Series *Cis*-$Ru(Bpy)_2L_2^{2+}$. *Inorg. Chem.* **1983**, *10*, 2444–2453. https://doi.org/10.1021/ic00159a021.

(79) Alary, F.; Heully, J.-L.; Bijeire, L.; Vicendo, P. Is the ^{3}MLCT the Only Photoreactive State of Polypyridyl Complexes? *Inorg. Chem.* **2007**, *46*, 3154–3165. https://doi.org/10.1021/ic062193i.

(80) Salassa, L.; Garino, C.; Salassa, G.; Gobetto, R.; Nervi, C. Mechanism of Ligand Photodissociation in Photoactivable $[Ru(Bpy)_2L_2]^{2+}$ Complexes: A Density Functional Theory Study. *J. Am. Chem. Soc.* **2008**, *130*, 9590–9597. https://doi.org/10.1021/ja8025906.

(81) Salassa, L.; Garino, C.; Salassa, G.; Nervi, C.; Gobetto, R.; Lamberti, C.; Gianolio, D.; Bizzarri, R.; Sadler, P. J. Ligand-Selective Photodissociation from $[Ru(Bpy)(4AP)_4]^{2+}$: A Spectroscopic and Computational Study. *Inorg. Chem.* **2009**, *48*, 1469–1481. https://doi.org/10.1021/ic8015436.

(82) Salassa, L.; Borfecchia, E.; Ruiu, T.; Garino, C.; Gianolio, D.; Gobetto, R.; Sadler, P. J.; Cammarata, M.; Wulff, M.; Lamberti, C. Photo-Induced Pyridine Substitution in *Cis*-$[Ru(Bpy)_2(Py)_2]Cl_2$: A Snapshot by Time-Resolved X-Ray Solution Scattering. *Inorg. Chem.* **2010**, *49*, 11240–11248. https://doi.org/10.1021/ic102021k.

(83) Camilo, M. R.; Cardoso, C. R.; Carlos, R. M.; Lever, A. B. P. Photosolvolysis of *Cis*-$[Ru(\alpha\text{-Diimine})_2(4\text{-Aminopyridine})_2]^{2+}$ Complexes: Photophysical, Spectroscopic, and Density Functional Theory Analysis. *Inorg. Chem.* **2014**, *53*, 3694–3708. https://doi.org/10.1021/ic5000205.

(84) Greenough, S. E.; Roberts, G. M.; Smith, N. A.; Horbury, M. D.; McKinlay, R. G.; Żurek, J. M.; Paterson, M. J.; Sadler, P. J.; Stavros, V. G. Ultrafast Photo-Induced Ligand Solvolysis of *Cis*-$[Ru(Bipyridine)_2(Nicotinamide)_2]^{2+}$: Experimental and Theoretical Insight into Its Photoactivation Mechanism. *Phys. Chem. Chem. Phys.* **2014**, *16*, 19141–19155. https://doi.org/10.1039/C4CP02359E.

(85) Tu, Y.-J.; Mazumder, S.; Endicott, J. F.; Turro, C.; Kodanko, J. J.; Schlegel, H. B. Selective Photodissociation of Acetonitrile Ligands in Ruthenium Polypyridyl Complexes Studied by Density Functional Theory. *Inorg. Chem.* **2015**, *54*, 8003–8011. https://doi.org/10.1021/acs.inorgchem.5b01202.

(86) Nisbett, K.; Tu, Y.-J.; Turro, C.; Kodanko, J. J.; Schlegel, H. B. DFT Investigation of Ligand Photodissociation in $[Ru^{II}(Tpy)(Bpy)(Py)]^{2+}$ and $[Ru^{II}(Tpy)(Me_2Bpy)(Py)]^{2+}$ Complexes. *Inorg. Chem.* **2018**, *57*, 231–240. https://doi.org/10.1021/acs.inorgchem.7b02398.

(87) Bahreman, A.; Limburg, B.; Siegler, M. A.; Bouwman, E.; Bonnet, S. Spontaneous Formation in the Dark, and Visible Light-Induced Cleavage, of a Ru–S Bond in Water: A Thermodynamic and Kinetic Study. *Inorg. Chem.* **2013**, *52*, 9456–9469.

https://doi.org/10.1021/ic401105v.

(88) Göttle, A. J.; Alary, F.; Boggio-Pasqua, M.; Dixon, I. M.; Heully, J.-L.; Bahreman, A.; Askes, S. H. C.; Bonnet, S. Pivotal Role of a Pentacoordinate ^{3}MC State on the Photocleavage Efficiency of a Thioether Ligand in Ruthenium(II) Complexes: A Theoretical Mechanistic Study. *Inorg. Chem.* **2016**, *55*, 4448–4456. https://doi.org/10.1021/acs.inorgchem.6b00268.

(89) Howerton, B. S.; Heidary, D. K.; Glazer, E. C. Strained Ruthenium Complexes Are Potent Light-Activated Anticancer Agents. *J. Am. Chem. Soc.* **2012**, *134*, 8324–8327. https://doi.org/10.1021/ja3009677.

(90) Wachter, E.; Glazer, E. C. Mechanistic Study on the Photochemical "Light Switch" Behavior of $[Ru(Bpy)_2Dmdppz]^{2+}$. *J. Phys. Chem. A* **2014**, *118*, 10474–10486. https://doi.org/10.1021/jp504249a.

(91) Havrylyuk, D.; Heidary, D. K.; Nease, L.; Parkin, S.; Glazer, E. C. Photochemical Properties and Structure-Activity Relationships of Ru(II) Complexes with Pyridylbenzazole Ligands as Promising Anticancer Agents. *Eur. J. Inorg. Chem.* **2017**, 1687–1694. https://doi.org/10.1002/ejic.201601450.

(92) Kohler, L.; Nease, L.; Vo, P.; Garofolo, J.; Heidary, D. K.; Thummel, R. P.; Glazer, E. C. Photochemical and Photobiological Activity of Ru(II) Homoleptic and Heteroleptic Complexes Containing Methylated Bipyridyl-Type Ligands. *Inorg. Chem.* **2017**, *56*, 12214–12223. https://doi.org/10.1021/acs.inorgchem.7b01642.

(93) Cuello-Garibo, J.-A.; Meijer, M. S.; Bonnet, S. To Cage or to Be Caged? The Cytotoxic Species in Ruthenium-Based Photoactivated Chemotherapy Is Not Always the Metal. *Chem. Commun.* **2017**, *53*, 6768–6771. https://doi.org/10.1039/C7CC03469E.

(94) Cuello-Garibo, J.-A.; James, C. C.; Siegler, M. A.; Hopkins, S. L.; Bonnet, S. Selective Preparation of a Heteroleptic Cyclometallated Ruthenium Complex Capable of Undergoing Photosubstitution of a Bidentate Ligand. *Chem. - Eur. J.* **2019**, *25*, 1260–1268. https://doi.org/10.1002/chem.201803720.

(95) Meijer, M. S.; Bonnet, S. Diastereoselective Synthesis and Two-Step Photocleavage of Ruthenium Polypyridyl Complexes Bearing a Bis(Thioether) Ligand. *Inorg. Chem.* **2019**, *58*, 11689–11698. https://doi.org/10.1021/acs.inorgchem.9b01669.

(96) Azar, D. F.; Audi, H.; Farhat, S.; El-Sibai, M.; Abi-Habib, R. J.; Khnayzer, R. S. Phototoxicity of Strained Ru(II) Complexes: Is It the Metal Complex or the Dissociating Ligand? *Dalton Trans.* **2017**, *46*, 11529–11532. https://doi.org/10.1039/C7DT02255G.

(97) Li, G.; Brady, M. D.; Meyer, G. J. Visible Light Driven Bromide Oxidation and Ligand Substitution Photochemistry of a Ru Diimine Complex. *J. Am. Chem. Soc.* **2018**, *140*, 5447–5456. https://doi.org/10.1021/jacs.8b00944.

(98) Roque III, J.; Havrylyuk, D.; Barrett, P. C.; Sainuddin, T.; McCain, J.; Colón, K.; Sparks, W. T.; Bradner, E.; Monro, S.; Heidary, D.; Cameron, C. G.; Glazer, E. C.; McFarland, S. A. Strained, Photoejecting Ru(II) Complexes That Are Cytotoxic Under Hypoxic Conditions. *Pho-*

tochem. Photobiol. **2020**, *96*, 327–339. https://doi.org/10.1111/php.13174.

(99) Kazlauskas, R. J.; Wrighton, M. S. Application of Rapid-Scan Fourier Transform Infrared Spectroscopy to Characterize the Monodentate Intermediate in the Photochemical Formation of Tetracarbonyl(4,4'-Dialkyl-2,2'-Bipyridine)Metal from Hexacarbonylmetal. *J. Am. Chem. Soc.* **1982**, *104*, 5784–5786. https://doi.org/10.1021/ja00385a039.

(100) Jones, W. E.; Smith, R. A.; Abramo, M. T.; Williams, M. D.; Van Houten, J. Photochemistry of Hetero-Tris-Chelated Ruthenium(II) Polypyridine Complexes in Dichloromethane. *Inorg. Chem.* **1989**, *28*, 2281–2285. https://doi.org/10.1021/ic00311a008.

(101) Tachiyashiki, S.; Nakamaru, K.; Mizumachi, K. A Long-Lived Intermediate with a Unidentate Dmbpy Ligand in the Photosubstitution of $[Ru(Bpy)_2(Dmbpy)]^{2+}$ (Dmbpy=3,3'-Dimethyl-2,2'-Bipyridine). *Chem. Lett.* **1992**, 1119–1122.

(102) Tachiyashiki, S.; Ikezawa, H.; Mizumachi, K. Identification of an Intermediate of the Photosubstitution of a Ruthenium(II) Diimine Complex With a Monodentate Chelating Ligand: ^{1}H NMR and HPLC Evidence. *Inorg. Chem.* **1994**, *33*, 623–625. https://doi.org/10.1021/ic00082a001.

(103) Arakawa, R.; Tachiyashiki, S.; Matsuo, T. Detection of Reaction Intermediates: Photosubstitution of (Polypyridine)Ruthenium(II) Complexes Using Online Electrospray Mass Spectrometry. *Anal. Chem.* **1995**, *67*, 4133–4138. https://doi.org/10.1021/ac00118a016.

(104) Thompson, D. W.; Wishart, J. F.; Brunschwig, B. S.; Sutin, N. Efficient Generation of the Ligand Field Excited State of Tris-(2,2'-Bipyridine)-Ruthenium(II) through Sequential Two-Photon Capture by $[Ru(Bpy)_3]^{2+}$ or Electron Capture by $[Ru(Bpy)_3]^{3+}$. *J. Phys. Chem. A* **2001**, *105*, 8117–8122. https://doi.org/10.1021/jp011854o.

(105) Welby, C. E.; Rice, C. R.; Elliott, P. I. P. Unambiguous Characterization of a Photoreactive Ligand-Loss Intermediate. *Angew. Chem. Int. Ed.* **2013**, *52*, 10826–10829. https://doi.org/10.1002/anie.201304219.

(106) Scattergood, P. A.; Ross, D. A. W.; Rice, C. R.; Elliott, P. I. P. Labilizing the Photoinert: Extraordinarily Facile Photochemical Ligand Ejection in an $[Os(N\hat{}N)_3]^{2+}$ Complex. *Angew. Chem. Int. Ed.* **2016**, *55*, 10697–10701. https://doi.org/10.1002/anie.201604959.

(107) Scattergood, P. A.; Khushnood, U.; Tariq, A.; Cooke, D. J.; Rice, C. R.; Elliott, P. I. P. Photochemistry of $[Ru(Pytz)(Btz)_2]^{2+}$ and Characterization of a κ^1-Btz Ligand-Loss Intermediate. *Inorg. Chem.* **2016**, *55*, 7787–7796. https://doi.org/10.1021/acs.inorgchem.6b00782.

(108) Scattergood, P. A.; Elliott, P. I. P. An Unexpected Journey from Highly Tunable Phosphorescence to Novel Photochemistry of 1,2,3-Triazole-Based Complexes. *Dalton Trans.* **2017**, *46*, 16343–16356. https://doi.org/10.1039/C7DT03836D.

(109) Findlay, J. A.; Barnsley, J. E.; Gordon, K. C.; Crowley, J. D. Synthesis and Light-Induced Actuation of Photo-Labile 2-Pyridyl-1,2,3-Triazole Ru(Bis-Bipyridyl) Appended Ferrocene Rotors. *Molecules* **2018**, *23*, 2037. https://doi.org/10.3390/molecules23082037.

(110) Welby, C. E.; Armitage, G. K.; Bartley, H.; Wilkinson, A.; Sinopoli, A.; Uppal, B. S.;

Rice, C. R.; Elliott, P. I. P. Photochemistry of Ru(II) 4,4′-Bi-1,2,3-Triazolyl (Btz) Complexes: Crystallographic Characterization of the Photoreactive Ligand-Loss Intermediate *Trans*-$[Ru(Bpy)(\kappa^2\text{-Btz})(\kappa^1\text{-Btz})(NCMe)]^{2+}$. *Chem. - Eur. J.* **2014**, *20*, 8467–8476. https://doi.org/10.1002/chem.201402354.

(111) Welby, C. E.; Grkinic, S.; Zahid, A.; Uppal, B. S.; Gibson, E. A.; Rice, C. R.; Elliott, P. I. P. Synthesis, Characterisation and Theoretical Study of Ruthenium 4,4′-Bi-1,2,3-Triazolyl Complexes: Fundamental Switching of the Nature of S_1 and T_1 States from MLCT to MC. *Dalton Trans.* **2012**, *41*, 7637–7646. https://doi.org/10.1039/c2dt30510k.

(112) Dixon, I. M.; Heully, J.-L.; Alary, F.; Elliott, P. I. P. Theoretical Illumination of Highly Original Photoreactive ^{3}MC States and the Mechanism of the Photochemistry of Ru(II) Tris(Bidentate) Complexes. *Phys. Chem. Chem. Phys.* **2017**, *19*, 27765–27778. https://doi.org/10.1039/C7CP05532C.

(113) Soupart, A.; Alary, F.; Heully, J.-L.; Dixon, I. M. On the Possible Coordination of a ^{3}MC State Itself? Mechanistic Investigation Using DFT-Based Methods. *Inorganics* **2020**, *8*, 15. https://doi.org/doi:10.3390/inorganics8020015.

(114) Soupart, A.; Alary, F.; Heully, J.-L.; Elliott, P. I. P.; Dixon, I. M. Exploration of Uncharted ^{3}PES Territory for $[Ru(Bpy)_3]^{2+}$: A New ^{3}MC Minimum Prone to Ligand Loss Photochemistry. *Inorg. Chem.* **2018**, *57*, 3192–3196. https://doi.org/10.1021/acs.inorgchem.7b03229.

(115) Soupart, A.; Alary, F.; Heully, J.-L.; Elliott, P. I. P.; Dixon, I. M. Recent Progress in Ligand Photorelease Reaction Mechanisms: Theoretical Insights Focusing on Ru(II) ^{3}MC States. *Coord. Chem. Rev.* **2020**, *408*. https://doi.org/10.1016/j.ccr.2020.213184.

(116) Aihara, Y.; Sato, K.; Shinozaki, K. Optical Resolution, Determination of Absolute Configuration, and Photoracemization of *Cis*-$RuL_2(CN)_2$ (L = 2,2′-Bipyridine and Its Analogues). *Inorg. Chem.* **2016**, *55*, 8387–8395. https://doi.org/10.1021/acs.inorgchem.6b00772.

(117) Asahara, M.; Kurimoto, H.; Nakamizu, M.; Hattori, S.; Shinozaki, K. H/D Solvent Isotope Effects on the Photoracemization Reaction of Enantiomeric the Tris(2,2′-Bipyridine)Ruthenium(II) Complex and Its Analogues. *Phys. Chem. Chem. Phys.* **2020**, *22*, 6361–6369. https://doi.org/10.1039/C9CP06758B.

(118) Ding, L.; Chung, L. W.; Morokuma, K. Excited-State Proton Transfer Controls Irreversibility of Photoisomerization in Mononuclear Ruthenium(II) Monoaquo Complexes: A DFT Study. *J. Chem. Theory Comput.* **2014**, *10*, 668–675. https://doi.org/10.1021/ct400982r.

(119) Rojas Pérez, Y.; Slep, L. D.; Etchenique, R. *Cis–Trans* Interconversion in Ruthenium(II) Bipyridine Complexes. *Inorg. Chem.* **2019**, *58*, 11606–11613. https://doi.org/10.1021/acs.inorgchem.9b01485.

(120) Crutchley, R. J.; Lever, A. B. P. Comparative Chemistry of Bipyrazyl and Bipyridyl Metal Complexes: Spectroscopy, Electrochemistry and Photoanation. *Inorg. Chem.* **1982**, *21*, 2276–2282. https://doi.org/10.1021/ic00136a030.

(121) Allen, G. H.; White, R. P.; Rillema, D. P.; Meyer, T. J. Synthetic Control of Excited-State

Properties. Tris-Chelate Complexes Containing the Ligands 2,2'-Bipyrazine, 2,2'-Bipyridine, and 2,2'-Bipyrimidine. *J. Am. Chem. Soc.* **1984**, *106*, 2613–2620. https://doi.org/10.1021/ja00321a020.

(122) Kalyanasundaram, K. Direct Observation of Substitutional Photochemistry in Tris(Bipyrazyl)Ruthenium(II). *J. Phys. Chem.* **1986**, *90*, 2285–2287. https://doi.org/10.1021/j100402a003.

(123) Ross, H. B.; Boldaji, M.; Rillema, D. P.; Blanton, C. B.; White, R. P. Photosubstitution in Tris Chelate Complexes of Ruthenium(II) Containing the Ligands 2,2'-Bipyrazine, 2,2'-Bipyrimidine, 2,2'-Bipyridine, and 4,4'-Dimethyl-2,2'-Bipyridine: Energy Gap Control. *Inorg. Chem.* **1989**, *28*, 1013–1021. https://doi.org/10.1021/ic00305a007.

(124) Masschelein, A.; Jacquet, L.; Kirsch-De Mesmaeker, A.; Nasielski, J. Ruthenium Complexes with 1,4,5,8-Tetraazaphenanthrene. Unusual Photophysical Behavior of the Tris-Homoleptic Compound. *Inorg. Chem.* **1990**, *29*, 855–860. https://doi.org/10.1021/ic00329a056.

(125) Welby, C. E.; Armitage, G. K.; Bartley, H.; Sinopoli, A.; Uppal, B. S.; Elliott, P. I. P. Photochemical Ligand Ejection from Non-Sterically Promoted Ru(II)Bis(Diimine) 4,4′-Bi-1,2,3-Triazolyl Complexes. *Photochem. Photobiol. Sci.* **2014**, *13*, 735–738. https://doi.org/10.1039/C3PP50437A.

(126) Lo, W. K. C.; Huff, G. S.; Cubanski, J. R.; Kennedy, A. D. W.; McAdam, C. J.; McMorran, D. A.; Gordon, K. C.; Crowley, J. D. Comparison of Inverse and Regular 2-Pyridyl-1,2,3-Triazole "Click" Complexes: Structures, Stability, Electrochemical, and Photophysical Properties. *Inorg. Chem.* **2015**, *54*, 1572–1587. https://doi.org/10.1021/ic502557w.

(127) Lee, C.; Yang, W.; Parr, R. G. Development of the Colle-Salvetti Correlation-Energy Formula into a Functional of the Electron Density. *Phys. Rev. B* **1988**, *37*, 785–789.

(128) Becke, A. D. Density-functional Thermochemistry. III. The Role of Exact Exchange. *J. Chem. Phys.* **1993**, *98*, 5648–5652. https://doi.org/10.1063/1.464913.

(129) Grimme, S.; Antony, J.; Ehrlich, S.; Krieg, H. A Consistent and Accurate Ab Initio Parametrization of Density Functional Dispersion Correction (DFT-D) for the 94 Elements H-Pu. *J. Chem. Phys.* **2010**, *132*, 154104. https://doi.org/10.1063/1.3382344.

(130) Grimme, S.; Ehrlich, S.; Goerigk, L. Effect of the Damping Function in Dispersion Corrected Density Functional Theory. *J. Comput. Chem.* **2011**, *32*, 1456–1465. https://doi.org/10.1002/jcc.21759.

(131) Andrae, D.; Haeussermann, U.; Dolg, M.; Stoll, H.; Preuss, H. Energy-Adjusted Ab Initio Pseudopotentials for the Second and Third Row Transition Elements. *Theor. Chim. Acta* **1990**, *77*, 123–141.

(132) Weigend, F.; Ahlrichs, R. Balanced Basis Sets of Split Valence, Triple Zeta Valence and Quadruple Zeta Valence Quality for H to Rn: Design and Assessment of Accuracy. *Phys. Chem. Chem. Phys.* **2005**, *7*, 3297–3305. https://doi.org/10.1039/b508541a.

(133) Poynton, F. E.; Bright, S. A.; Blasco, S.; Williams, D. C.; Kelly, J. M.; Gunnlaugsson, T.

The Development of Ruthenium(II) Polypyridyl Complexes and Conjugates for *in Vitro* Cellular and *in Vivo* Applications. *Chem. Soc. Rev.* **2017**, *46*, 7706–7756. https://doi.org/10.1039/C7CS00680B.

(134) McKenzie, L. K.; Bryant, H. E.; Weinstein, J. A. Transition Metal Complexes as Photosensitisers in One- and Two-Photon Photodynamic Therapy. *Coord. Chem. Rev.* **2019**, *379*, 2–29. https://doi.org/10.1016/j.ccr.2018.03.020.

(135) Penfold, T. J.; Gindensperger, E.; Daniel, C.; Marian, C. M. Spin-Vibronic Mechanism for Intersystem Crossing. *Chem. Rev.* **2018**, *118*, 6975–7025. https://doi.org/10.1021/acs.chemrev.7b00617.

(136) Harvey, J. N.; Aschi, M.; Schwarz, H.; Koch, W. The Singlet and Triplet States of Phenyl Cation. A Hybrid Approach for Locating Minimum Energy Crossing Points between Non-Interacting Potential Energy Surfaces. *Theor. Chem. Acc.* **1998**, *99*, 95–99.

(137) Harvey, J. N. Spin-Forbidden Reactions: Computational Insight into Mechanisms and Kinetics: Spin-Forbidden Reactions. *Wiley Interdiscip. Rev. Comput. Mol. Sci.* **2014**, *4*, 1–14. https://doi.org/10.1002/wcms.1154.

(138) Zhang, J.; Zhang, X.; Suarez-Alcantara, K.; Jennings, G.; Kurtz, C. A.; Lawson Daku, L. M.; Canton, S. E. Resolving the Ultrafast Changes of Chemically Inequivalent Metal–Ligand Bonds in Photoexcited Molecular Complexes with Transient X-Ray Absorption Spectroscopy. *ACS Omega* **2019**, *4*, 6375–6381. https://doi.org/10.1021/acsomega.8b03688.

(139) Hollebone, B. R.; Langford, C. H.; Serpone, N. The Mechanisms of Photoreactivity of Coordination Compounds: Limiting Cases of Decay on a Specific Nuclear Coordinate (DOSENCO) or via Random Coordinate Selection (DERCOS). *Coord. Chem. Rev.* **1981**, *39*, 181–224. https://doi.org/10.1016/S0010-8545(00)80514-7.

(140) Vanquickenborne, L. G.; Ceulemans, A. Ligand-Field Models and the Photochemistry of Coordination Compounds. *Coord. Chem. Rev.* **1983**, *48*, 157–202. https://doi.org/10.1016/0010-8545(83)80002-2.

(141) Wernet, Ph.; Kunnus, K.; Josefsson, I.; Rajkovic, I.; Quevedo, W.; Beye, M.; Schreck, S.; Grübel, S.; Scholz, M.; Nordlund, D.; Zhang, W.; Hartsock, R. W.; Schlotter, W. F.; Turner, J. J.; Kennedy, B.; Hennies, F.; de Groot, F. M. F.; Gaffney, K. J.; Techert, S.; Odelius, M.; Föhlisch, A. Orbital-Specific Mapping of the Ligand Exchange Dynamics of $Fe(CO)_5$ in Solution. *Nature* **2015**, *520*, 78–81. https://doi.org/10.1038/nature14296.

(142) Orr-Ewing, A. J. Taking the Plunge: Chemical Reaction Dynamics in Liquids. *Chem. Soc. Rev.* **2017**, *46*, 7597–7614. https://doi.org/10.1039/C7CS00331E.

(143) Durham, B.; Wilson, S. R.; Hodgson, D. J.; Meyer, T. J. *Cis-Trans* Photoisomerization in $Ru(Bpy)_2(OH_2)_2^{2+}$. Crystal Structure of *Trans*-$[Ru(Bpy)_2(OH_2)(OH)](ClO_4)_2$. *J. Am. Chem. Soc.* **1980**, *102*, 600–607.

(144) Drolet, D. P.; Lees, A. J. Photochemistry of $(Eta^5\text{-}C_5H_5)Rh(CO)_2$ in Phosphine Solutions: Evidence for an Associative Photosubstitution Mechanism. *J. Am. Chem. Soc.* **1990**, *112*, 5878–

5879. https://doi.org/10.1021/ja00171a037.

(145) Mukuta, T.; Simpson, P. V.; Vaughan, J. G.; Skelton, B. W.; Stagni, S.; Massi, M.; Koike, K.; Ishitani, O.; Onda, K. Photochemical Processes in a Rhenium(I) Tricarbonyl N-Heterocyclic Carbene Complex Studied by Time-Resolved Measurements. *Inorg. Chem.* **2017**, *56*, 3404–3413. https://doi.org/10.1021/acs.inorgchem.6b02936.

(146) Portius, P.; Yang, J.; Sun, X.-Z.; Grills, D. C.; Matousek, P.; Parker, A. W.; Towrie, M.; George, M. W. Unraveling the Photochemistry of $Fe(CO)_5$ in Solution: Observation of $Fe(CO)_3$ and the Conversion between $^3Fe(CO)_4$ and $^1Fe(CO)_4$(Solvent). *J. Am. Chem. Soc.* **2004**, *126*, 10713–10720. https://doi.org/10.1021/ja048411t.

(147) Besora, M.; Carreón-Macedo, J.-L.; Cowan, A. J.; George, M. W.; Harvey, J. N.; Portius, P.; Ronayne, K. L.; Sun, X.-Z.; Towrie, M. A Combined Theoretical and Experimental Study on the Role of Spin States in the Chemistry of $Fe(CO)_5$ Photoproducts. *J. Am. Chem. Soc.* **2009**, *131*, 3583–3592. https://doi.org/10.1021/ja807149t.

(148) Lomont, J. P.; Nguyen, S. C.; Harris, C. B. Ultrafast Infrared Studies of the Role of Spin States in Organometallic Reaction Dynamics. *Acc. Chem. Res.* **2014**, *47*, 1634–1642. https://doi.org/10.1021/ar500032d.

(149) Kunnus, K.; Josefsson, I.; Rajkovic, I.; Schreck, S.; Quevedo, W.; Beye, M.; Weniger, C.; Grübel, S.; Scholz, M.; Nordlund, D.; Zhang, W.; Hartsock, R. W.; Gaffney, K. J.; Schlotter, W. F.; Turner, J. J.; Kennedy, B.; Hennies, F.; de Groot, F. M. F.; Techert, S.; Odelius, M.; Wernet, Ph.; Föhlisch, A. Identification of the Dominant Photochemical Pathways and Mechanistic Insights to the Ultrafast Ligand Exchange of $Fe(CO)_5$ to $Fe(CO)_4$EtOH. *Struct. Dyn.* **2016**, *3*, 043204. https://doi.org/10.1063/1.4941602.

(150) Mukuta, T.; Tanaka, S.; Inagaki, A.; Koshihara, S.; Onda, K. Direct Observation of the Triplet Metal-Centered State in $[Ru(Bpy)_3]^{2+}$ Using Time-Resolved Infrared Spectroscopy. *ChemistrySelect* **2016**, *1*, 2802–2807. https://doi.org/10.1002/slct.201600747.

For Table of Contents Only

SYNOPSIS TOC

A full road map is provided for the multistep mechanism of photoinduced ligand loss from tris(diimine) Ru(II) complexes and formation of bis(solvento) *cis* and *trans* photoproducts. Two major pathways have been identified; one involves two sequential photonic excitations through the formation of an intermediate mono(solvento) product (red route). The other is a novel one-photon pathway (blue route) in which ligand dechelation, coordination of solvent and ligand loss all occur in the triplet excited state.

TOC GRAPHIC